A Desorption Electrospray Ionization Mass Spectrometry Imaging Approach to Monitor Toxic Ionic Liquids in Zebrafish (*Danio rerio*)

Consuelo Javiera Perez

A thesis submitted to the Faculty of Graduate Studies in partial fulfillment of the Master of Science in Chemistry

Graduate Program in Chemistry

Centre for Research in Mass Spectrometry

York University

Toronto, Canada

August 2016

Acknowledgments

I would like to take this opportunity to thank those who were involved in my academic journey. Firstly, thank you to my supervisor Professor Demian Ifa for his advice and guidance throughout my time as a graduate student and for giving me the chance to be a part of the field of mass spectrometry. I am tremendously grateful for my supervisory committee members, Professor Derek Wilson and Professor Diethard Bohme for their direction and advice every year during research evaluations and MS-ESE seminars. Thanks to Professor Mark Bayfield for agreeing to be a part of the examination committee.

A special and warm thank you to Dr. Alessandra Tata for patiently mentoring and training me in the field of mass spectrometry; her knowledge and direction were pivotal to my success. She helped anyway possible, proofreading research evaluation papers, presentations, orals and she was always open for meaningful conversations. I would like to thank all present and past colleagues and friends in Professor Ifa's research group: Dragos Lostun, Michel L. De Campos, Paulo Yamasaki, Irina Oleganyanski, Amin Khatami, Rachel Fu, Aida Khanbabakhani, Rogerio Castro, Danilo Rodrigues, Karen Cipriano, Shamina Prova, Aafreen Baga and all members of the Centre for Research in Mass Spectrometry. I would also like to thank my dear friends and fellow chemistry graduate students, Nicholas Tulsiram and Chris Schruder for their help and advice.

I'm grateful to my wonderful family for motivating and supporting me to pursue academia. I'm endlessly grateful for the sacrifices my mother has made towards her career and personal life to raise my sister and I on her own in a foreign country. My endurance, strength and perseverance are a mere reflection of yours. Lastly, thanks to my sister for somehow knowing me better than I know myself.

Once again, thank you to all who took part in this unforgettable journey.

Abstract

Ambient mass spectrometry imaging has become an increasingly powerful technique for the direct analysis of biological tissues in the open environment with minimal sample preparation and fast analyses times. In this study, we introduce desorption electrospray ionization mass spectrometry imaging (DESI-MSI) as a novel, rapid and sensitive approach to monitor toxic ionic liquids in zebrafish (*Danio rerio*). AMMOENG 130, distearyldimethylammonium chloride, is used as a surfactant in commercialized personal care products. AMMOENG 130 is toxic to zebrafish exhibiting an LC_{50} of 5.2 mg/L, causing extensive damage to gill secondary lamellae and increasing membrane permeability. Zebrafish were exposed to AMMOENG 130 in a static 96 hour acute toxicity study in concentrations below and near the LC_{50} ranging from 1.25-5.0 mg/L. DESI-MS analysis of zebrafish gills revealed the appearance of a metabolite in all concentrations of exposure. The metabolite was further characterized with a high resolution hybrid LTQ-Oritrap mass spectrometer as the stearyltrimethylammonium ion of *m/z* 312. Whole body zebrafish tissue from exposure concentrations were mapped for AMMOENG 130 and its dealkylated metabolite, accumulation was mainly found in the nervous and respiratory systems suggesting that AMMOENG 130 and its metabolite were capable of penetrating the blood brain barrier of zebrafish brain uncovering potential neurotoxic effects. To evaluate DESI-MS as a potential environmental IL monitoring tool, AMMOENG 130 was spotted in varying concentrations onto PTFE surfaces and the limit of detection found was 10 µg/L. Hence, we demonstrate here the simultaneous characterization, accumulation and metabolism of a toxic IL in whole body zebrafish analyzed by DESI-MSI. This ambient ionization mass spectrometry technique shows great promise for the direct analysis of biological tissues to monitor toxic and persistent environmental pollutants in aquatic organisms for qualitative analysis with future potential for quantitative analysis.

Table of Contents iv-v

Appendix

List of Figures

List of Tables

List of Abbreviations

AIMS	Ambient Ionization Mass Spectrometry
a.u.	Arbitrary units (manufacturer's unit)
BBB	Blood brain barrier
CID	Collision Induced dissociation
CCAC	Canadian Committee on Animal Care
CYP	Cytochrome P_{450}
DART-MS	Direct Analysis in Real Time Mass Spectrometry
DESI-MS	Desorption Electrospray Ionization Mass Spectrometry
DESI-MSI	Desorption Electrospray Ionization Mass Spectrometry Imaging
EC_{50}	Half maximal effective concentration
EI	Electron Impact
ESI-MS	Electrospray Ionization Mass Spectrometry
IL(s)	Ionic iquid(s)
HRMS	High resolution mass spectrometry
LC_{50}	Half maximum lethal concentration
LOD(s)	Limit(s) of detection
LOQ(s)	Limit(s) of quantitation
MS	Mass Spectrometry/Mass spectrometer
MS-222	Tricaine methanesulphonate
MS/MS	Mass Spectrometry/Mass Spectrometry (Tandem Mass Spectrometry)
OECD	Organization for Economic Co-operation and Development
DPDA	Phase Doppler Particle Analysis
Psi	Pounds per square inch
PC(s)	Phosphatidylcholine(s)
PCP(s)	Personal care product(s)
PTFE	Polytetrafluoroethylene

REACh	European Registration Evaluation Authorization and restriction of Chemicals
TIC	Total ion count
VOC	Volatile organic compounds
YACC	York University's Animal Care Committee

Chapter I

Introduction

1.1. Ambient Ionization Mass Spectrometry

Ambient Ionization Mass Spectrometry (AIMS) is a subdivision of Mass Spectrometry (MS) techniques that allows the ionization of compounds to take place under standard atmospheric pressure conditions before it is introduced into the mass spectrometer inlet for detection. This broad family of techniques does not require extensive sample preparation in probing surfaces of various sizes and shapes in gas, liquid and solid phases.[1] This enables the sample to be interrogated in its native-state without the need for preservation, sampling before analysis or chemical separation techniques. The introduction of Desorption Electrospray Ionization Mass Spectrometry (DESI-MS) by Cooks et al. in 2004[2] and Direct Analysis in Real Time Mass Spectrometry (DART-MS) by Cody et al. in 2005[6] were pivotal advancements that revolutionized the field of Mass Spectrometry.[1] After both techniques were introduced many other ambient ionization mass spectrometry techniques began to surface quite quickly. AIMS techniques have been grouped and described based on the nature of desorption/ionization process: spray or jet-based, plasma-based, heat/laser assisted desorption/ionization, acoustic, etc. A vast amount of AIMS techniques have been discovered and implemented starting from 2004.

Table 1 Ambient ionization methods

	Method name	Acronym	Agent	Characteristics	Reference
1	Desorption electrospray ionization	DESI	Sprays	Imaging capabilities, reactive mode, small (<500 Da) and large molecules	29
2	Easy ambient sonic-spray ionization	EASI	Sprays	Imaging capabilities, small (<500 Da) molecules	30
3	Desorption ionization by charge exchange	DICE	Sprays, chemical ionization	Small (<500 Da) molecules	31
4	Transmission mode desorption electrospray ionization	TM-DESI	Sprays	Reactive mode	32
5	Nanospray-desorption/electrospray ionization	Nano-DESI	Sprays	Imaging capabilities, small (<500 Da) and large molecules	33
6	Probe electrospray ionization	PESI	Sprays	Imaging capabilities, small (<500 Da) and large molecules	34
7	Liquid microjunction-surface sampling probe	LMJ-SSP	Sprays	Imaging capabilities, reactive mode, small (<500 Da) molecules	35
8	Paper spray	PS	Sprays	Reactive mode, small (<500 Da) and large molecules	36
9	Direct analysis in real time	DART	Plasmas	Small (<500 Da) and large molecules	37
10	Low-temperature plasma probe	LTP	Plasmas	Reactive mode, small (<500 Da) molecules	38
11	Flowing atmospheric pressure afterglow	FAPA	Plasmas	Small (<500 Da) molecules	39
12	Desorption atmospheric pressure chemical ionization	DAPCI	Plasmas	Small (<500 Da) molecules	40
13	Desorption corona beam ionization	DCBI	Plasmas	Small (<500 Da) molecules	41
14	Dielectric barrier discharge ionization	DBDI	Plasmas	Small (<500 Da) molecules	42
15	Electrospray-assisted laser desorption ionization	ELDI	Lasers, sprays	Imaging capabilities, small (<500 Da) and large molecules	43
16	Laser ablation electrospray ionization	LAESI	Lasers, sprays	Imaging capabilities, small (<500 Da) molecules	44
17	Laser-assisted desorption electrospray ionization	LADESI	Lasers, sprays	Imaging capabilities, small (<500 Da) and large molecules	45
18	Laser desorption electrospray ionization	LDESI	Lasers, sprays	Imaging capabilities, small (<500 Da) and large molecules	46
19	Laser-induced acoustic desorption-electrospray ionization	LIAD-ESI	Lasers, acoustic, sprays	Small (<500 Da) and large molecules	47

(*Continued*)

Table 1 (*Continued*)

	Method name	Acronym	Agent	Characteristics	Reference
20	Neutral desorption extractive electrospray ionization	ND-EESI	Sprays	Reactive mode, small (<500 Da) molecules	48
21	Radiofrequency acoustic desorption and ionization	RADIO	Sprays, acoustic	Small (<500 Da) molecules	49
22	Atmospheric pressure solids analysis probe	ASAP	Heat, plasmas	Small (<500 Da) molecules	50
23	Infrared laser ablation metastable-induced chemical ionization	IR-LAMICI	Lasers, chemical ionization	Small (<500 Da) and large molecules	51
24	Rapid evaporative ionization mass spectrometry	REIMS	Chemical ionization	Heating, small (<500 Da) molecules	52
25	Desorption atmospheric pressure photoionization	DAPPI	Chemical ionization	Photons as proton source, small (<500 Da) molecules	53
26	Beta electron-assisted direct chemical ionization	BADCI	Chemical ionization	Beta particles as proton source, small (<500 Da) molecules	54
27	Extractive electrospray ionization	EESI	Sprays	Reactive mode, small (<500 Da) and large molecules	55
28	Remote analyte sampling transport and ionization relay	RASTIR	Sprays	Small (<500 Da) and large molecules	56
29	Laser ablation flowing atmospheric-pressure afterglow	LA-FAPA	Plasmas	Small (<500 Da) molecules	57
30	Surface activated chemical ionization	SACI	Plasmas	Small (<500 Da) molecules	58
31	Single-particle aerosol mass spectrometry	SPAMS	Lasers	Small (<500 Da) molecules	59
32	Laser diode thermal desorption	LDTD	Lasers, plasmas	Small (<500 Da) molecules	60
33	Helium atmospheric pressure glow discharge ionization	HAPGDI	Plasmas	Small (<500 Da) molecules	61
34	Surface acoustic wave nebulization	SAWN	Acoustic	Small (<500 Da) molecules	62
35	Ultrasonication-assisted spray ionization	UASI	Acoustic	Small (<500 Da) and large molecules	63
36	Atmospheric pressure-thermal desorption/electrospray ionization	AP-TD/ESI	Heat, sprays	Small (<500 Da) molecules	64
37	Microplasma discharge ionization	Microplasma	Plasmas	Small (<500 Da) molecules	65
38	Atmospheric pressure thermal desorption ionization	APTDI	Heat	Small (<500 Da) molecules	66
39	Desorption electrospray/metastable-induced ionization	DEMI	Sprays, plasmas	Small (<500 Da) molecules	67
40	Switched ferroelectric plasma ionizer	SwiFerr	Plasmas	Small (<500 Da) molecules	68
41	Laser electrospray mass spectrometry	LEMS	Lasers, sprays	Small (<500 Da) and large molecules	69
42	Plasma-assisted desorption ionization	PADI	Plasmas	Small (<500 Da) molecules	70

Figure 1: Ambient Desorption Ionization Mass Spectrometry Techniques. Reprinted with permission from reference [7].

All AIMS techniques allow complex samples to be analyzed with high throughput capabilities, high sensitivity and rapid analysis times in comparison to other MS techniques such as liquid chromatography- mass spectrometry (LC-MS) or gas chromatography- mass spectrometry (GC-MS) techniques that require sample pre-treatment, liquid-liquid extractions, solid-phase extractions and chemical derivatizations before analysis. The integrity of the sample from its native state is destroyed and can no longer be assessed without modifications. One of the most

explored AIMS techniques is DESI-MS, researchers around the world have dedicated their lives' work on the instrumentation, ionization mechanisms, applications and development of DESI-MS and DESI-MS imaging.

1.2. DESI-MS and DESI-MS Imaging

DESI-MS is an ambient ionization mass spectrometry technique developed by Professor Graham R. Cooks from Purdue University in 2004. DESI has been categorized as a soft ionization technique, such that it does not produce extensive fragmentation as opposed to traditional mass spectrometry ionization techniques like Electron Impact (EI). In DESI, a stream of charged solvent droplets driven by a nitrogen gas and high voltage impacts the sample surface. A thin liquid film is produced by primary solvent microdroplets by which analytes on the surface are dissolved. Subsequent droplet collisions on the surface discharge secondary droplets. Secondary microdroplets containing the analytes are delivered to the mass spectrometer through the mass spectrometer inlet. Further droplet reduction produces gas-phase ion molecules by couloumbic explosions and evaporation described by the ion evaporation or charge residue mechanisms, as in conventional electrospray ionization (ESI) of analytes in bulk solution.[7] Ion formation in DESI was proposed to occur by the droplet pickup mechanism under ambient conditions (Figure 2).

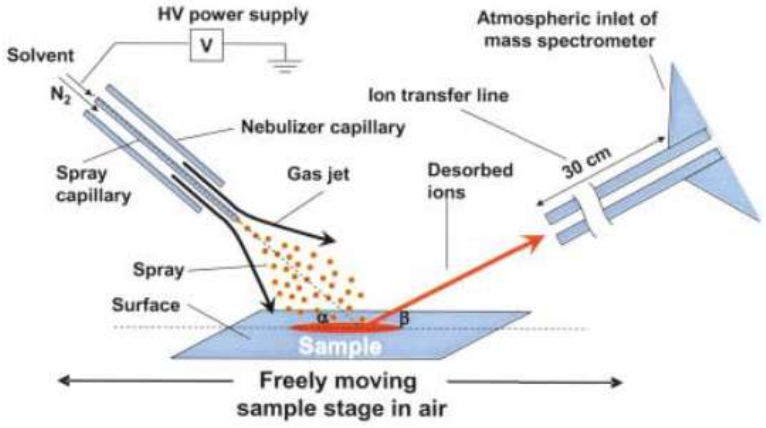

Figure 2: Schematic of the ambient ionization process in DESI-MS. The spray solvent and nebulizing gas mobilize through the capillary with an applied voltage. The electrospray charged solvent impacts the sample surface and the ionization takes place in ambient conditions.

Desorbed analyte ions are directed towards the MS inlet. Reprinted with permission from reference [2].

The mechanism of ion formation in DESI has been proposed through the droplet pickup model. Investigations using phase Doppler particle analysis (DPDA) have provided evidence of the physical characteristics of the DESI spray before and after the spray impacts the sample surface. Measurements of the sizes and velocities of the droplets produced in the DESI sprayer under standard operating DESI parameters (flow rate: 2 µL/min, spray solvent of methanol/water (1:1), gas pressure 160 psi, spray incident angle of 60°). Droplets were measured at a 2 mm distance from the sprayer tip, impacting primary droplets had velocities between 100-200 m/s and an average size of 2-4 µm. PDPA measurements of droplet sizes and velocities at multiple heights from the impact site demonstrated that after droplets impact the surface, small and fast droplets move at shallow angles with respective to the surface.[8]

The droplet pickup model in DESI has been simulated by computational fluid dynamics providing convincing evidence of the transport and collision processes that occur. The theoretical computational fluid dynamics simulations agreed well with the experimental DESI PDPA experiments in terms of particle sizes and their respective velocities.[1, 3]

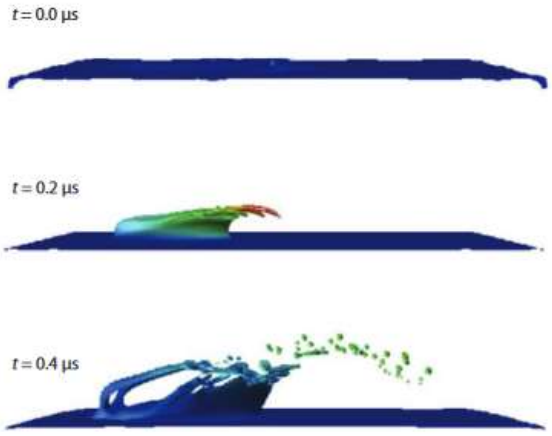

Figure 3: Multiphase computational fluid dynamics simulations of the droplet collisions in the thin film at t=0 before impact and at time t= 0.2 µs and t=0.4 µs after impact with a spray to surface angle of 55°. In the simulation, the primary droplet velocity in blue indicates the fluid at

rest, while red constitutes the fluid at maximum velocity. Reprinted with permission from reference [3].

It was found that droplets leaving the impact site contained the liquid originating from the surface and from the incident droplet providing a strong basis for the two step droplet pickup mechanism. Computational fluid dynamics simulations described the mechanism to occur in three consecutive stages: (1) the formation of a thin liquid film on the sample surface by impacting droplets, (2) extraction of the solid phase analytes into the thin film, (3) collision of the primary droplets with the thin film, producing secondary droplets containing the analyte.[8, 9]

In terms of instrumentation, DESI consists of several geometric parameters. These geometric parameters must be optimized for efficient desorption and ionization of the analytes of interest. The incident angle (α), the collection angle (β), tip to surface distance (d_1), MS inlet to surface distance (d_2), and the horizontal distance from the capillary tip to MS inlet can be manipulated to increase sensitivity, selectivity, signal stability and intensity (Figure 4).[10] The choice of the solvent spray plays a major role in desorption compared to the DESI ion source parameters. The analytes of interest are not detected efficiently or at all unless dissolved and desorbed from the surface by a suitable solvent spray, regardless of the DESI ion source parameter optimization. The most crucial role of the solvent spray is to solubilize, desorb and aid in the ionization of the analytes of interest for DESI-MS detection.

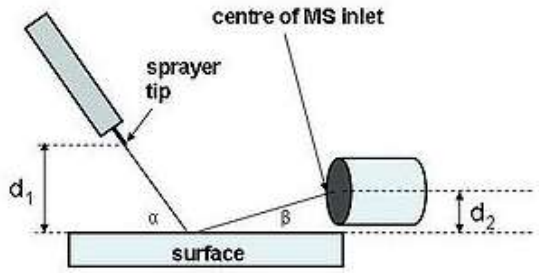

Figure 4: Schematic representation of the DESI ion source parameters for optimization. The incident angle (α), the collection angle (β), spray tip to surface distance (d_1), MS inlet to surface distance (d_2), and horizontal distance from capillary tip to MS inlet (not shown). Reprinted and modified with permission from reference [10].

Typical ranges of operation for DESI source parameters are described in Table 1. The wide ranges of the DESI source parameters are a result of variations in the optimization of the desorption and ionization of analytes of interest in different surface types and matrices of complex analyte mixtures.

Table 1: Typical DESI Source Parameters

Parameter	Range
Nebulizing gas pressure	80-160 Psi
Solvent flow rate	1-5 µL/min.
Spray voltage	2-6 kV
Incident angle	30-70°
Sprayer to surface distance	1-5 mm
Sprayer to MS inlet	1-8 mm
MS inlet desolvation temperature	200-300°C

In the last decade, DESI-MS imaging has become an attractive tool for the spatially resolved identification of chemical compounds in biological tissues. A software-controlled 2D moving stage is coupled to the DESI ion source that rasters across the sample surface in the x and y direction to direct the tissue for simultaneous MS analysis.[11-14] The moving stage is incorporated below the DESI ion source setup to produce ion images of signal intensity versus spatial coordinates of the sampling area. To create 2D DESI-MS images, an area of interest is chosen for imaging and the sample is placed onto a target surface. PMMA, PTFE coated microscopic glass slides, porous PTFE, and PTFE sheets are typical surfaces used for DESI-MS imaging of dried liquid samples.[5] For biological tissue analysis, the tissue is cryosectioned, mounted onto microscopic glass slides and analyzed in its native-state without further manipulation.

When DESI-MS is used in imaging modality, developments and applications are multifaceted and have been explored in the field of lipidomics,[11, 12, 15] metabolomics,[16-18] drug discovery[16] cancer typification[11, 19] and forensics.[20, 21] It has infinite applications and capabilities for accurate compound identification, mapping chemical specific distributions and aiding in the discovery of compounds' biological significance.[22] DESI-MS has not only been useful for qualitative analysis but has also been investigated on its suitability for quantitative analysis.[5, 23] Endogenous biomarker and drug-induced accumulation are emerging areas of research evaluated by DESI-MS imaging for the specific distribution of drugs and metabolites in animal organs and whole body tissues.[18, 23] Likewise, exogenous compounds have also been mapped in whole body mice and locusts by DESI-MS imaging.[24, 25] From our research group, this technique was successful in mapping endogenous fatty acids and multiple subclasses of phospholipids ranging from phosphatidylserines, phosphatidylinositols, and sulfatides in whole body zebrafish in negative mode. Phospholipids were distributed in the brain and spinal cord fish tissue. The bile salt 5α-cyprinol 27-sulfate was confined to the gastrointestinal system of the fish.[26]

1.3. Ionic Liquids and Ionic Liquid Toxicity to Aquatic Organisms

Ionic liquids (ILs) are organic or semi organic salts composed of a cation and anion moiety which are liquids at or below room temperature with low melting points usually below 100°C. ILs have desirable physiochemical properties for the development of greener solvent alternatives to conventional organic solvents including high thermal and chemical stability, non-flammability and non-volatility.[27] ILs have negligible vapour pressures and cannot generate volatile organic compounds (VOCs) in the atmosphere causing unwanted air pollution, for this reason ILs have attracted large attention as media for greener synthesis and solvent alternatives. ILs have been implemented as lubricants, performance additives, biocatalysts and solvents for organic synthesis, stationary and mobile phases for chromatography separation.[28] Because ILs are composed of an anionic and cationic moiety the possibilities of different combinations to tailor physiochemical properties for a specific purpose are endless. Cation moieties include

ammonium, phosphonium, pyrrolidinium, imidazolium, pyridinium, morpholinium and piperidinium with various combinations of alkyl side chain lengths, side chain functionalization and anion. Anion moieties are typically small inorganic molecules such as halides, phosphates, perfluorinated or cyano-based anions to larger organic molecules such as tosylate.

Despite their infinite combinations and wide applicability, commonly used ILs have been found to exhibit higher toxicities than traditional organic solvents. The viability of these compounds as green solvents has been under scrutiny for quite some time due to toxic effects on aquatic organisms. Consequently, the release of toxic ILs into aquatic ecosystems poses a high threat for the environment and human health such that toxic effects elicited may cause acute or chronic toxicity, sedimentation or bioaccumulation.[29] IL acute toxicities have been tested and some of LC_{50} values for ILs were substantially lower than for common organic solvents such as methanol (LC_{50} 12,700 – 29,400 mg/L), acetonitrile (LC_{50} >100 mg/L), and dichloromethane (LC_{50} >100 mg/L).[4] Acute toxicity tests have been performed on different species such as marine luminescent bacteria (*Vibrio fischeri*),[30-32] the limnic green algae (*Scenedesmus vascuolatus*),[33] the freshwater plant (*Lemna minor*),[32] the freshwater crustacean (*Daphnia magna*),[33-35] and zebrafish (*Danio rerio*)[4, 33, 36] to assess toxicity from multiple IL subclasses. In a study from 2009, three freshwater aquatic organisms from different trophic levels, the algae *P. subcapitata* (primary producer), the freshwater flea *Daphnia magna* (primary consumer) and the zebrafish *Danio rerio* (predator) were assessed for acute toxicities of ILs containing different positively charged head groups: imidazolium, pyridinium, pyrrolidinium, morpholinium, ammonium, sulfonium and thiophenium. Generally, the more toxic compounds were long chain quaternary ammonium based ILs to the algae, flea and zebrafish while very low toxicities were found for sulfonium and morpholinium based ILs. The long chain quaternary ammonium compounds tested were AMMOENG 100 and AMMOENG 130, these ILs were classified based on hazard ranking from Passino and Smith in 1987 (Table 2).

Table 2: IL Hazard Ranking from Passino and Smith Published in 1987

Hazard Ranking	Toxicity range (EC_{50})
Practically harmless	100-1000 mg/L
Slightly toxic	10-100 mg/L
Moderately toxic	1-10 mg/L
Highly toxic	0.1-1 mg/L

In algae, AMMOENG 100 and AMMOENG 130 were classified as highly toxic with EC_{50} of 0.12 mg/L and EC_{50} of 0.83 mg/L, respectively. The freshwater flea, *Daphnia magna* exhibited an EC_{50} of 1.57 mg/L and 0.55 mg/L for AMMOENG 100 and AMMOENG 130, such were classified as moderately and highly toxic. In *Danio rerio*, AMMOENG 100 and AMMOENG 130 were classified as slightly toxic. In terms of species based IL toxicity, it has been suggested that fish appear to be less sensitive to IL toxicity compared to other species in lower trophic levels.[37] In general, the AMMOENG series: AMMOENG 100, 101, 102, 110, 111, 112, 120, and 130 are ILs structurally composed of tetrasubstituted-ammonium cations with varying saturated alkyl or oligo(ethylene glycol) chains and small anion moieties such as $[Cl]^-$, $[MeOSO_3]^-$, $[EtOSO_3]^-$ $[H_2PO_4]^-$, and $[MeCO_2]^-$.

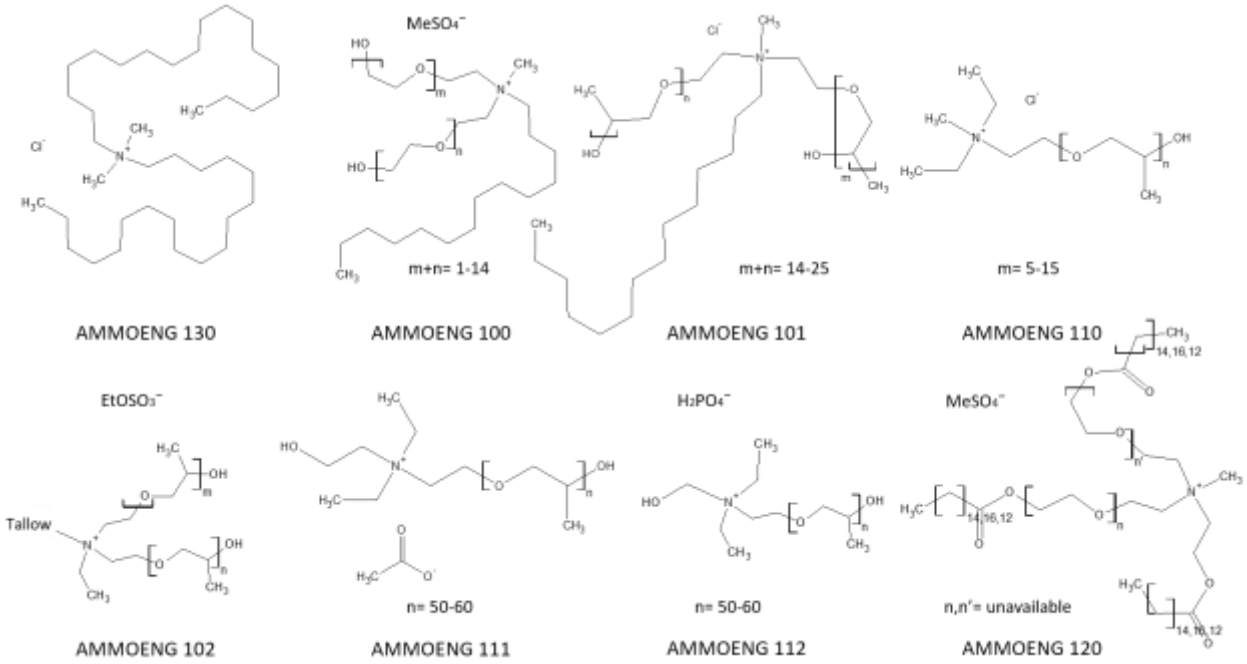

Figure 5: Structures of AMMOENG based ILs.

These ILs are available in large quantities, hence represent an interesting alternative to expensive and not readily available imidazolium based ILs. AMMOENG type ILs have gained attention due to their surfactant properties with use in commercial personal care products (PCPs) such as detergents and softeners.[38] Moreover, AMMOENG based ILs have been used for many years in industry as surfactants and most of them are already covered by European Registration Evaluation Authorization and restriction of Chemicals (REACh) legislation with the exception of AMMOENG 120 and AMMOENG 130.[39] Pretti and coworkers evaluated the acute toxicity for 15 common ILs by determining the LC_{50} in zebrafish (Figure 6).[4]

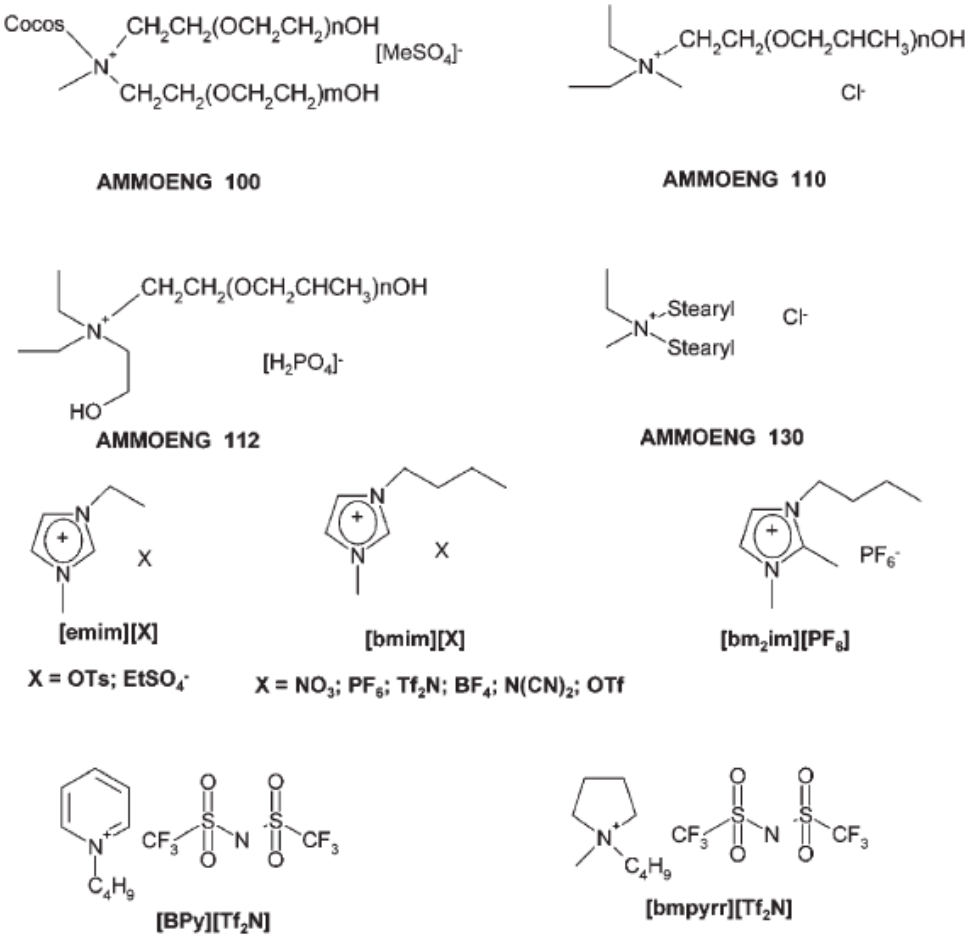

Figure 6: Ionic liquids tested for acute toxicity to the zebrafish. Reprinted with permission from reference [4].

Among the 15 ILs tested, all compounds exhibited toxicities above >100 mg/L considered practically harmless. Yet, AMMOENG 100 and AMMOENG 130 were found to be toxic with a median lethal concentration (LC_{50}) of 5.9 mg/L and 5.2 mg/L, respectively. Histopathological examination of the fish gill tissue revealed marked damage, enlargement and disorganization in secondary gill lamellae with disepithelialization in treated fish. Damage to the gill membranes was predicted to be a cause of altered and damaged lipid bilayers and consequently enhanced membrane permeability to external ions.[4, 33] Correlations between IL structure and toxicity have been made by many research groups where the majority of the ecotoxicological data focuses on the influence of the cation head groups, the alkyl side chain length, and the anion toxicity.[40] The two major contributors of toxicity is the cation head group and the alkyl side chain length. One of the major toxicity contributors originates from what has been called the "alkyl side chain effect" where long hydrophobic alkyl chains promote increased toxicity as the alkyl chain length increases.[32, 41] The influence on the alkyl side chain length was conducted on an imidazolium based IL; toxicity increased significantly with an EC_{50} of 115 µM for a C2 alkyl side chain length to EC_{50} of 3.5 µM for a C14 alkyl chain length. The toxicity remained relatively constant for increasing alkyl side chains after C14, the EC_{50} for a C16 alkyl side chain was 4.81 µM and 9.21 µM for C18, respectively.[42]

Independent of the organism and experimental method, ILs containing long alkyl chain lengths, highly hydrophobic or lipophilic significantly increased the observed toxicity. There is growing evidence that the toxic mechanism of action for lipophilic ILs is to penetrate, dissolve and disintegrate biological membranes affecting biological functions in cells. Therefore, ILs with long alkyl chains incorporate into phospholipid bilayers and alter the structural integrity of biological membranes.[4, 37] In organisms, lipophilic ILs are metabolized and eliminated only to a small degree, if at all, and hence have a large potential to bioaccumulate.[43] Acute toxicity in combination with chronic toxicity, sedimentation, and bioaccumulation are crucial endpoints that need to be determined for environmental risk assessment to meet regulatory standards and guidelines, and most importantly to encourage greener practices.[29, 44] By evaluating the toxicity of ILs and making correlations in regards to IL structure, more environmentally friendly

ILs can be synthesized to prevent bioaccumulation, toxicity, developmental and reproductive abnormalities in aquatic life in the environment.

1.4. Research Aims

The aim of this thesis project was to demonstrate that DESI-MSI, an ambient mass spectrometry technique, is suitable to monitor toxic ionic liquids in zebrafish. AMMOENG 130 has not been explored beyond its toxicity thus, provides an opportunity to investigate DESI-MS as a proof of principle study for AMMOENG 130 characterization, accumulation, metabolism and degradation in a model organism. IL environmental fate, and metabolic fate within organisms and toxic mechanisms of action are still not well understood especially for AMMOENG based ILs. Moreover, we sought out the viability of DESI-MSI as a potential quantitative monitoring tool for the analysis of toxic and persistent environmental pollutants. Ionic species are to some extent already partially dissociated in solution and therefore, charged before MS ionization processes providing enhanced chemical specificity and lower limits of detection (LOD). By evaluating analytical parameters such as the limit of detection, we can have a better understanding whether this technique shows promise for quantitative environmental applications and whether it can be an alternative tool to laborious and time consuming chromatography-interfaced mass spectrometry techniques such as liquid chromatography- mass spectrometry (LC-MS) and gas chromatography mass-spectrometry (GC-MS).

Chapter II

Experimental

This experimental chapter describes in detail the tests and methodologies conducted in order to characterize and monitor ILs in zebrafish by DESI-MSI. AMMOENG 130 was characterized by mass spectrometry to later monitor the IL in zebrafish tissue. Zebrafish were exposed to the IL in a static 96 hour test, in which behavioural and physical changes were noted during the study. Zebrafish gill tissue was analysed by DESI-MS where an AMMOENG 130 metabolite was found and characterized. In order to exclude the possibility of AMMOENG 130 degrading in the water a degradation study was conducted that mimicked the zebrafish exposure study. Later, a zebrafish gill extract was prepared and the metabolite was identified by a hybrid high resolution LTQ-Orbitrap. In order to investigate the accumulation of AMMOENG 130 and other species images of the whole body fish tissue were obtained by DESI-MSI. Sections 2.1 through 2.7 gives specific experimental guidelines and parameters for each individual experiment conducted.

2.1. Characterization of AMMOENG 130 by ESI-MS and ESI-MS/MS

To characterize AMMOENG 130, a Thermo Finnigan LTQ (San Jose, CA, USA) was used to collect IL spectra with an ESI source in the mass range of *m/z* 200-1000. A standard solution of 10 mg/mL of AMMOENG 130 in chloroform was serially diluted with methanol to 100 ng/mL. A solution of AMMOENG 100 was prepared at the same concentration. ESI-MS experimental conditions consisting of a voltage of 3 kV, a nitrogen gas pressure of 100 psi and a flow rate of 5 µL/min of pure methanol was used for all experiments. Collision-induced dissociation (CID) was performed for AMMOENG 130 standard using energies between 20-30% with a mass range of *m/z* 200-750.

2.2 AMMOENG 130 Exposure Study to the Zebrafish

A 96 hour IL exposure study was performed in accordance to the regulations for the care and management of fish set by the Canadian Committee on Animal Care (CCAC) and York University's

Animal Care Committee (YACC) and the Economic Co-operation and Development (OECD): Fish Acute Toxicity Test No. 203. Four zebrafish were placed in four polycarbonate 2L aquaria and were exposed to 0, 1.25, 2.50 and 5.0 mg/L of AMMOENG 130 by administering the IL into the tank rearing water. The water temperature was kept at 22 ± 1ºC and fish were kept under laboratory illumination in a 12-hour daily photoperiod. No food was administered during the study and fish were monitored periodically for physical and behaviour changes in intervals of 1, 3, 6, 12, 24, 48, 72, and 96 hours.

2.3. Zebrafish Sample Preparation and Cryosectioning

After the 96 hour exposure period, surviving zebrafish were euthanized with 300 mg/L of MS-222 solution. Zebrafish were thoroughly washed three times with distilled water upon removal from the euthanizing solution. Deceased fish were placed into flexible, peel away moulds for cryosectioning. A 5% CMC solution was prepared and poured into individual moulds containing a whole body zebrafish. Zebrafish CMC embedded blocks were used to prepare 50 µm tissue sections on a Shandon E cryotome from Thermo Scientific (Nepean, ON, CA). Tissue sections were placed on microscopic glass slides, kept in a -80°C and later in a -18˚C freezer for immediate use. Tissue sections were air dried for 20 minutes prior to DESI-MS imaging analysis.

2.4. DESI-MS and DESI-MS Imaging Acquisition Parameters

DESI-MS profiles of zebrafish gills on sections of whole body zebrafish tissue were acquired using a Thermo Scientific LTQ mass spectrometer (San Jose, CA, USA) equipped with a lab built DESI source and a 2D moving stage for imaging. The DESI ion source was assembled based on a prototype from Prosolia Inc., (Indianapolis, IN, USA) previously described.[45] DESI ion source parameters such as the capillary tip to surface distance, the mass spectrometer inlet to capillary tip distance and the incident angle were optimized for zebrafish tissue. An incident angle of 52°, 1 mm capillary tip to surface distance and a 3-5 mm distance from the mass inlet to the solvent capillary tip was used. A nitrogen gas pressure of 100 psi and a flow rate of 2 µL/min of pure

methanol was chosen for optimal desorption and ionization of AMMOENG 130 from 50 µm zebrafish tissue sections.

For DESI-MS imaging, the DESI ion source was mounted onto a 2D moving stage capable of moving in the x and y direction for image acquisition. A total of n=4 fish per concentration (control, 1.25, 2.5 and 5.0 mg/L) for a total of n=16 animals were analyzed for IL distribution. DESI-MS imaging of whole body zebrafish was performed in positive ion mode with pure methanol at a flow rate of 2 µL/min, the injection time was set to 150 ms and 3 microscans were summed. Tissue imaging experiments were performed with a 2D moving stage by collecting mass spectral data by continuously scanning in horizontal rows in the x direction with a velocity of 200-350 µm/s every 200 µm over a mass range of *m/z* 200-1000. The zebrafish tissue imaging dimensions ranged from 3-4 cm in width vs. 1-1.5 cm in length dependent upon the size of the tissue section under MS analysis. Imaging acquisition times varied between 1.5-2.5 hours with a spatial resolution of 200 µm for all images. The mass spectra were processed by Qual Browser Xcalibur 2.0 and ImageCreator ver. 3.0 software was used to convert the Xcalibur 2.0 mass spectra files (.raw) into a format compatible with BioMap (freeware, http://www.maldi-msi.org/). BioMap processed the mass spectral data to acquire 2D ion images of tissue surface coordinates versus IL ion signal intensity.

2.5. AMMOENG 130 Degradation Study

A degradation study similar to "Closed Bottle Tests" was conducted to assess the stability and degradation of AMMOENG 130 in water during 96 hours. AMMOENG 130 was placed in 250 mL capped bottles in concentrations of 1.25, 2.5 and 5.0 mg/L. A control with distilled water, but without the IL was run in parallel with total volumes of 200 mL. Instead of monitoring the depletion of dissolved molecular oxygen as in Closed Bottle Tests, 500 µL of the IL was directly infused in an ESI source coupled to the LTQ mass spectrometer. The IL was sampled from each concentration in 12 hour intervals for 96 hours for the detection of IL degradation products. The

ESI-MS parameters were kept constant as previously described for the characterization of AMMOENG 130 with the exception of the mass range. The mass spectral data was collected between *m/z* 200-700.

2.6. Metabolite Extraction and Identification with HRMS Analysis

Zebrafish extract was prepared and analyzed by ESI-MS and ESI-MS/MS via a high resolution hybrid linear ion trap-orbitrap mass spectrometer (LTQ-Orbitrap Elite, Thermo Scientific, USA) for metabolite identification. The zebrafish gill extract was prepared by manually removing a portion of the zebrafish gill tissue from the fish body. The gill tissue was grounded by a mortar and pestle, placed into a 1.5 mL Eppendorf tube, macerated and extracted with methanol. The extract was centrifuged at 7000 rpm for 30 minutes. The supernatant was separated, collected, and transferred into an Eppendorf tube. The supernatant was dried down in a concentrator for 2 hours until complete evaporation and resuspended in 400 µL of methanol.

For HRMS analysis, the ESI-MS operating parameters were the following: spray voltage was set to 4 kV, the capillary temperature to 250°C, the S-lens rf level to 68% and the flow rate to 5 µL/min. Full scan mass spectra of the gill extract were acquired in the mass range of *m/z* 200-1000. Tandem mass spectrometry (MS/MS) experiments were conducted by isolating the metabolite within ±0.01 Da with a collision energy of 50-51%.

2.7. DESI-MS Determination of the Limit of Detection of AMMOENG 130

10 mg of AMMOENG 130 dissolved in 10 mL chloroform was serially diluted to concentrations of 1 ng/L, 10 ng/L, 100 ng/L, 1 µg/L (data not shown), 10 µg/L, 100 µg/L, 1 mg/L, 10 mg/L and 100 mg/L in methanol. Each concentration of 1 µL was spotted onto PTFE coated microscopic glass slides and left to dry in the open air for approximately 10 minutes and thereafter analyzed by DESI-MS. DESI-MS spectra was collected for each spotted concentration to assess the limit of detection. DESI ion source parameters consisted of an incident angle of 52°, 1 mm capillary tip to

surface distance and 5 mm distance from the mass inlet to the solvent capillary tip. A nitrogen gas pressure of 100 psi and a flow rate of 3 µL/min of pure methanol was chosen for optimal desorption and ionization of AMMOENG 130.

Chapter III

Results and Discussion

3.1. Characterization of AMMOENG 130 via ESI-MS and ESI-MS/MS

To the best of our knowledge, AMMOENG 130 has not been previously analyzed by mass spectrometry therefore, the analysis of an AMMOENG 130 standard solution was performed by ESI-MS and ESI-MS/MS for characterization. The chemical formula for AMMOENG 130 is $[C_{38}H_{80}N][Cl]$ with a molecular weight of 586.5 g/mol. AMMOENG 130 was detected in positive ion mode as the molecular ion of *m/z* 551, $[C_{38}H_{80}N]^+$; ionic species of *m/z* 523, *m/z* 495, and *m/z* 312 were also detected in the ESI-MS spectrum, these ions were identified as hexadecylstearyldimethylammonium ion $[C_{36}H_{76}N]^+$, tetradecylstearyldimethylammonium ion/dihexadecyldimethylammonium ion $[C_{34}H_{72}N]^+$ and stearyltrimethylammonium ion $[C_{21}H_{46}N]^+$, respectively (Figure 7 and Figure 8a).

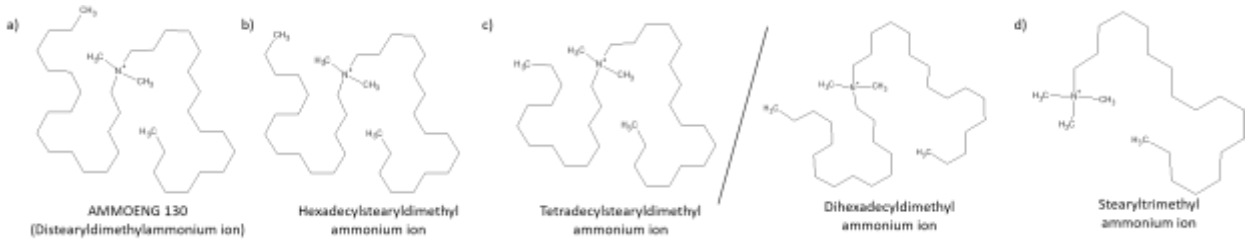

Figure 7: Chemical Structure of AMMOENG 130 and other ionic species in the IL standard. a) AMMOENG 130, distearyldimethylammonium ion, $[C_{38}H_{80}N]^+$ of *m/z* 551. b) Hexadecylstearyldimethylammonium ion, $[C_{36}H_{76}N]^+$ of *m/z* 523. c) Tetradecyldimethylstearylammonium ion, $[C_{34}H_{72}N]^+$ of *m/z* 495. d) Stearyltrimethylammonium ion, $[C_{21}H_{46}N]^+$ of *m/z* 312.

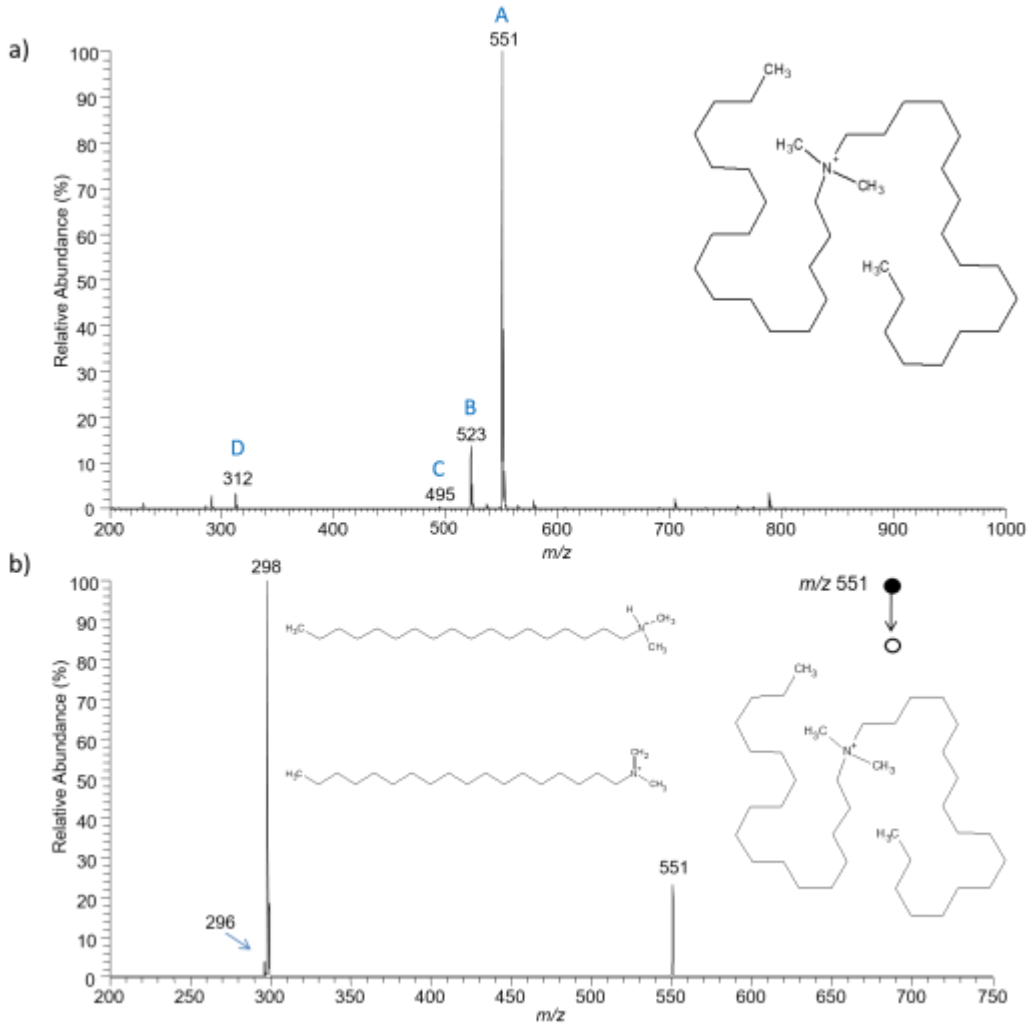

Figure 8: Characterization of AMMOENG 130. a) ESI-MS spectrum of AMMOENG 130. IL ions of *m/z* 551, 523, 495 and 312 corresponding to AMMOENG 130 molecular ion $[C_{38}H_{80}N]^+$, $[C_{36}H_{76}N]^+$, $[C_{34}H_{72}N]^+$, and $[C_{21}H_{46}N]^+$, respectively. b) ESI-MS/MS spectrum of AMMOENG 130 isolated and fragmented with a collision energy of 25% displaying two CID fragments of *m/z* 298 and *m/z* 296.

The monoisotopic AMMOENG 130 peak of *m/z* 551 was isolated and fragmented by collision-induced dissociation (CID) with an isolation window of 1 Da. MS/MS fragments of *m/z* 298 and *m/z* 296 were identified as $[C_{21}H_{44}N]^+$ and $[C_{20}H_{42}N]^+$ (Figure 8b). The most abundant fragment of *m/z* 298 arises from the loss of one of the C18 alkyl chains ($C_{18}H_{37}$) from the parent compound with a subsequent addition of hydrogen to the nitrogen atom. The MS/MS fragment of *m/z* 296 corresponds to the loss of the alkyl chain ($C_{18}H_{37}$) with the formation of carbon nitrogen double bond for increased stabilization (Figure 8b).

Subsequently, CID was conducted on other ionic species encountered in the ESI-MS full scan spectrum. AMMOENG 130 standard purchased was a greater than 95% purity standard, therefore the presence of other species in the mass spectrum was expected. The ion of *m/z* 523 was identified as hexadecylstearyldimethylammonium with fragments of *m/z* 298 and *m/z* 270. The fragment of *m/z* 298 is a common fragment in all the MS/MS spectra of ionic species. In this case, *m/z* 298 arises from the loss of the C16 alkyl chain with the gain of hydrogen. The ion of *m/z* 270 corresponds to the loss of the adjacent alkyl chain ($C_{18}H_{37}$) following the addition of hydrogen to the nitrogen atom (Figure 9).

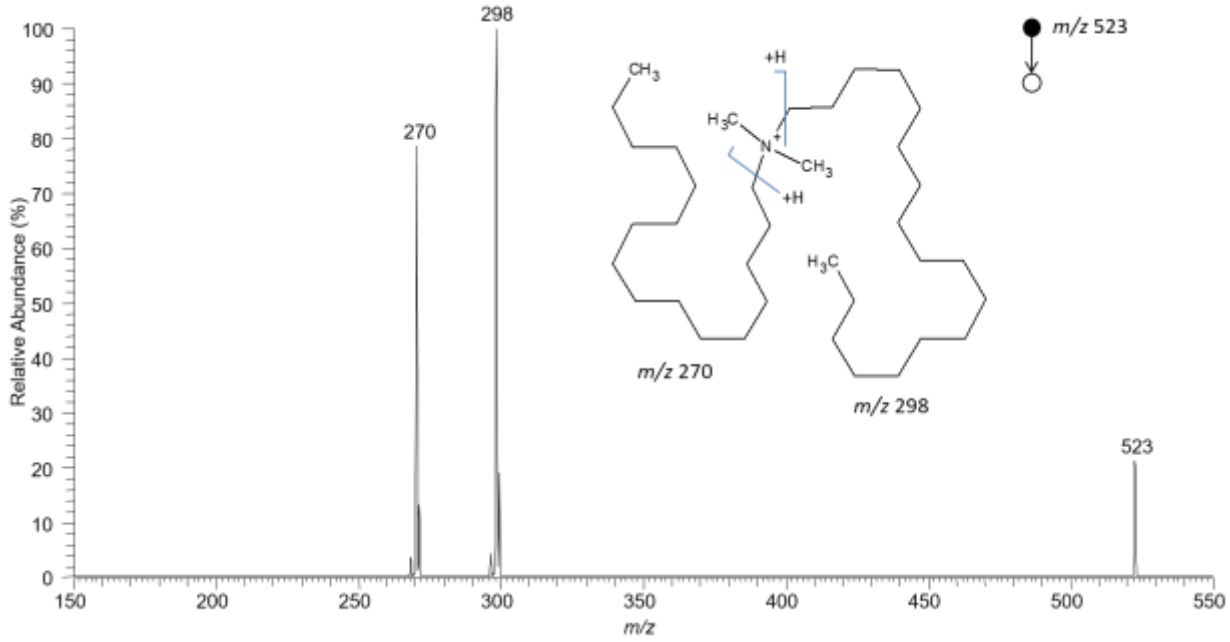

Figure 9: ESI-MS/MS spectrum of hexadecylstearyldimethylammonium ion, $[C_{36}H_{76}N]^+$ of *m/z* 522.6 with two major fragments of *m/z* 298 and *m/z* 270 using a collision energy of 25%.

The ion of *m/z* 495 was initially identified as tetradecylstearyldimethylammonium ion with fragments of *m/z* 270, *m/z* 298, *m/z* 268 and *m/z* 242 with chemical formula of $[C_{18}H_{40}N]^+$, $[C_{20}H_{44}N]^+$, $[C_{18}H_{38}N]^+$ and $[C_{16}H_{36}N]^+$, respectively (Figure 10). The fragment of *m/z* 270 corresponds to the loss of the C16 alkyl chain ($C_{16}H_{33}$) with subsequent addition of hydrogen to the molecule. The fragment of *m/z* 298 corresponds to the cleavage of $C_{14}H_{29}$ alkyl chain with an addition of hydrogen to the nitrogen atom. The fragment of *m/z* 242 arises from the cleavage of

$C_{18}H_{37}$ alkyl chain with an addition of hydrogen. Due to the fragmentation pattern, a mixture of tetradecylstearyldimethylammonium and dihexadecyldimethylammonium was evident. Tetradecylstearyldimethylammonium contains a C14 and a C18 alkyl chain, while dihexadecyldimethylammonium ion contains two C16 alkyl chains. The most intense fragment ion in the MS/MS spectrum is *m/z* 270 due to both C16 chains being cleaved from dihexadecyldimethylammonium ion.

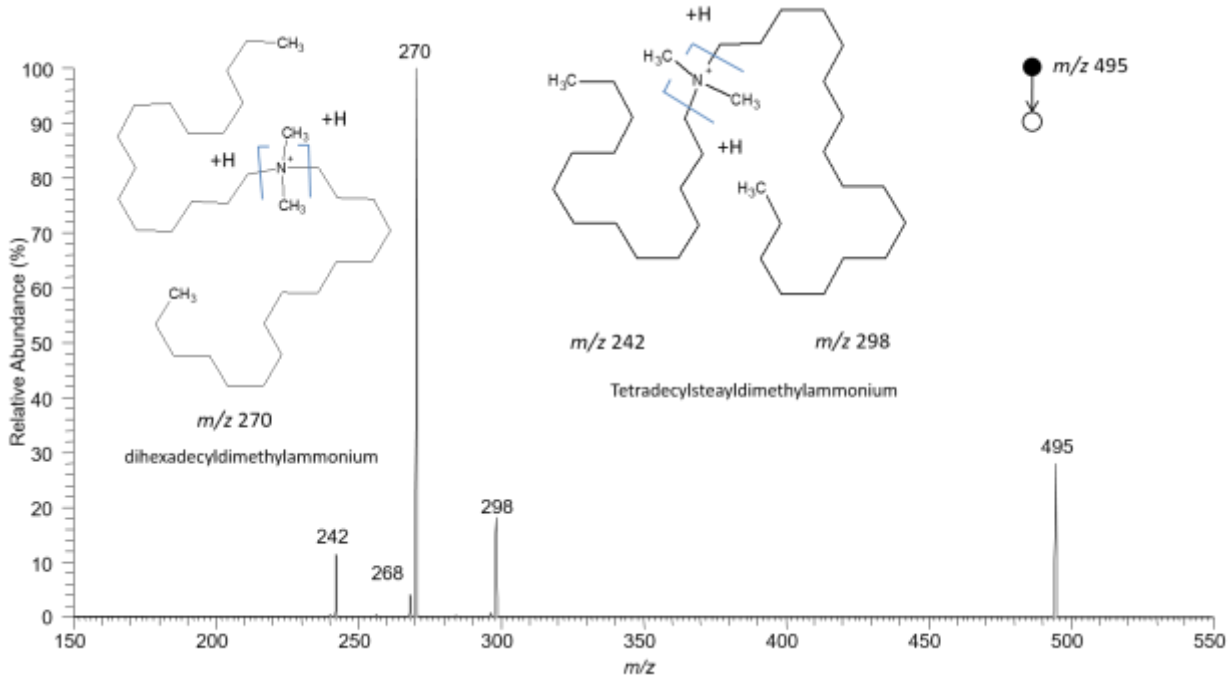

Figure 10: ESI-MS/MS spectrum of tetradecylstearyldimethylammonium/ dihexadecyldimethylammonium, $[C_{34}H_{72}N]^+$, of *m/z* 495 fragmented with a collisional energy of 30% displaying a major fragment of *m/z* 270 $[C_{18}H_{40}N]^+$ and 3 minor fragments of *m/z* 298 $[C_{20}H_{44}N]^+$, *m/z* 268 $[C_{18}H_{38}N]^+$ and *m/z* 242 $[C_{16}H_{36}N]^+$.

The ion of *m/z* 312 was identified as stearyltrimethylammonium ion with fragments of *m/z* 296, *m/z* 270 and *m/z* 185. The fragment of *m/z* 296 corresponds to the ion with chemical formula of $[C_{20}H_{42}N]^+$ (Figure 11).

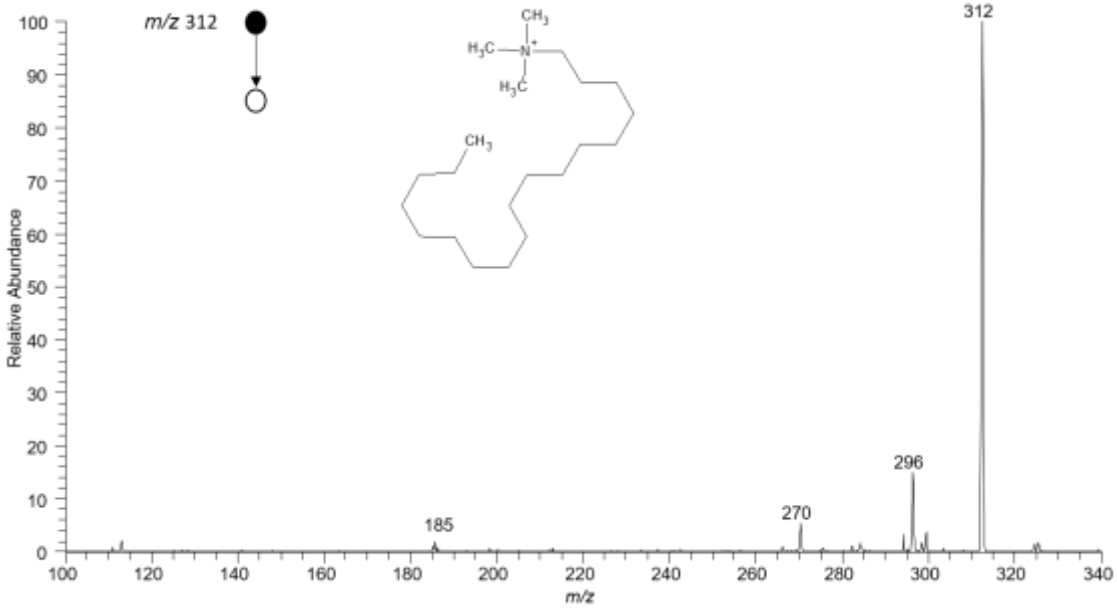

Figure 11: ESI-MS/MS spectrum of stearyltrimethylammonium ion, $[C_{21}H_{46}N]^+$ of *m/z* 312 fragmented with a collisional energy of 30% displaying fragments of *m/z* 296, *m/z* 270 and *m/z* 185.

Moreover, the characterization of AMMOENG 130 was performed on a high resolution LTQ-Orbitrap mass spectrometer for confirmation with the LTQ data. High resolution allowed for tentative identification of each peak with mass errors of less than 5 ppm. The summary of the high resolution LTQ-Orbitrap data can be found below in Table 3.

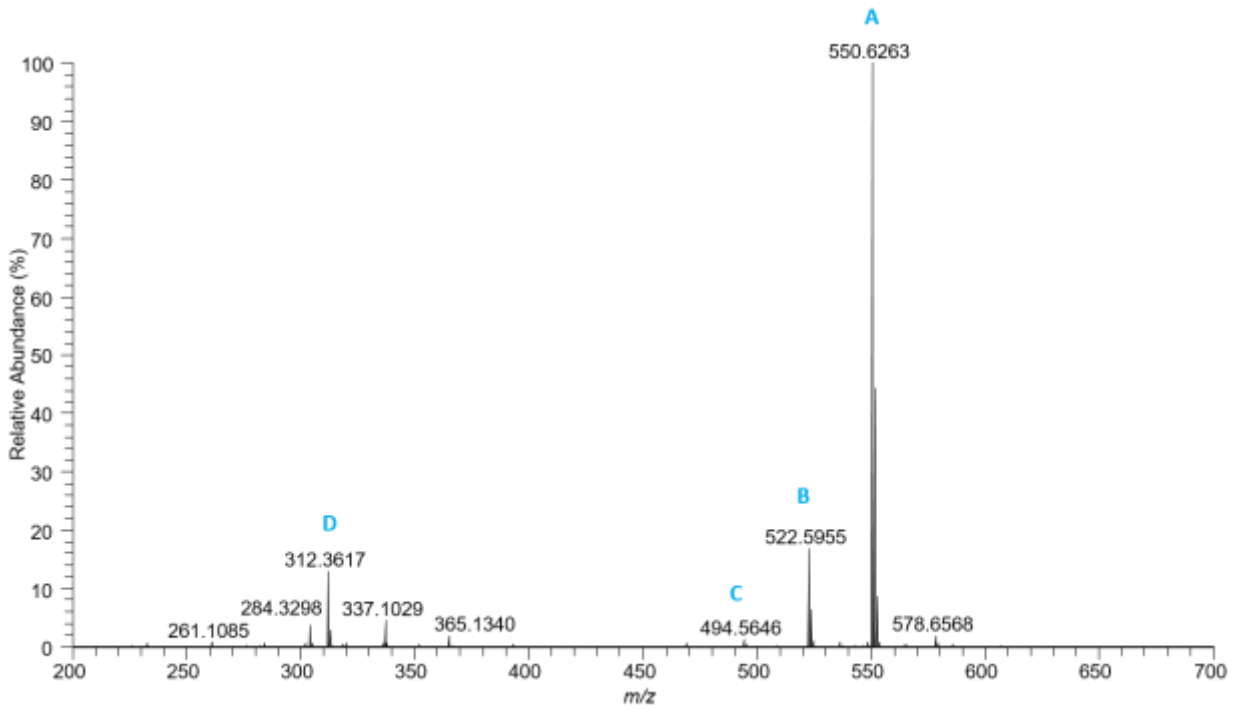

Figure 12: AMMOENG 130 standard solution of 10 ng/L analyzed by ESI-MS via a high resolution hybrid LTQ-Orbitrap Mass Spectrometer.

Table 3: Characterization of AMMOENG 130 Analyzed by a High Resolution Hybrid LTQ-Orbitrap Mass Spectrometer by ESI-MS and ESI-MS/MS

Ion	Ion Assignment	Monoisotopic mass	LTQ-Orbitrap (*m/z*)	Mass error (ppm)	CID fragments (*m/z*)
A	AMMOENG 130	550.6291	550.6263	5.0	298.3463, 296.3308
B	Hexadecylstearyldimethyl ammonium ion	522.5978	522.5955	4.4	298.3456, 270.3145
C	Tetradecylstearyldimethyl ammonium ion/ Dihexadecyldimethylammonium ion	494.5665	494.5646	3.6	270.3144, 298.3461, 242.2837
D	Trimethylstearyl ammonium ion	312.3632	312.3615	4.8	296.3303, 280.2627, 206.2352, 132.5990

The ESI-MS/MS spectra of ions A through D gathered from the hybrid LTQ-Orbitrap instrument can be found in Appendix A. In addition to the characterization of AMMOENG 130, a full scan ESI-MS spectrum in positive ion mode was collected from a standard solution of AMMOENG 100. A mixture of ILs was detected due to different lengths of the alkyl chains where the ethylene glycol subunits in both chains range from m+n= 1-14. Further experiments were not conducted with AMMOENG 100, yet the ESI-MS spectrum can be found in Appendix C.

3.2. Zebrafish Exposure and Mortality

The animals were exposed to AMMOENG 130 for 96 hours to induce accumulation. AMMOENG 130 was administered into the tank water containing four fish at concentrations of 1.25, 2.5 and 5.0 mg/L. Zebrafish were monitored for mortality, overt visible physical and behavioural changes compared to control during the exposure period (Table 4).

Table 4: Mortality, Physical and Behavioural Changes in Zebrafish to AMMOENG 130 Exposure during 96 hours.

AMMOENG 130 concentration (mg/L)	Physical Changes	Behavioural Changes	Zebrafish Mortality
Control (0)	N/A	N/A	96 hours-euthanized
1.25	Gill redness and inflammation Epidermal discoloration Abdominal distension	General reduction in activity Lack of swimming Spurs of erratic/ rapid swimming	96 hours-euthanized
2.5	Gill redness and inflammation Epidermal discoloration	N/A	Death - 12 >24 hours
5.0	Gill redness and inflammation Epidermal discoloration	N/A	Death - 12 >24 hours

During the first 12 hours, fish in all concentrations demonstrated normal behaviour compared to control. Zebrafish exposed to 5.0 mg/L and 2.5 mg/L were found deceased only after 24 hours as a result of the highly toxic concentrations near the LC_{50}. Deceased fish displayed signs of epidermal discoloration, inflammation of the buccal cavity and gills. Some fish exposed to both

these concentrations exhibited severe abdominal distension and inflammation. The fish abdomen was visibly distended beyond its normal girth (Figure 13b).

Figure 13: Zebrafish Acute Toxicity Study. a) Deceased fish in tanks of 2.5 mg/L of AMMOENG 130. b) Whole body zebrafish embedded in CMC moulds displaying a distended and swollen abdomen from an exposure concentration of 5.0 mg/L of AMMOENG 130. c) CMC embedded whole body zebrafish from concentrations of 5.0 mg/L (first and second column of fish) and 2.5 mg/L (third and fourth column of fish) displaying toxicity symptoms including distended abdomens, gill and buccal cavity redness and inflammation.

Inflammation and growth dilution are characteristic signs of acute toxicity and chemical excretion. Abdominal distension is a pseudo-elimination process by which substances are not

physically eliminated, however the concentration is diluted inside the organism by an increase in the fish tissue volume by fluid retention.[44] During 48-96 hours of the exposure study, fish in 1.25 mg/L displayed a general decrease in activity, staying motionless for large periods of time with spurs of rapid and erratic swimming compared to control.[4] Pretti and coworkers observed similar behavioural changes upon exposure to AMMOENG 130. Fish in the control group and those exposed to 1.25 mg/L survived the 96 hour study and were euthanized prior to DESI-MS analysis.

3.3. DESI-MS Analysis of Zebrafish Gills

Gills are the first point of contact and entry of water-borne contaminants into the fish from respiratory exchange, therefore the presence of the IL was investigated here. DESI-MS profiles were acquired for control zebrafish gills and a plethora of phospholipids, mainly phosphatidylcholines (PC) in the range of *m/z* 750-1000 were found (Figure 14). Chramow et al. and Lostun et al. have previously characterized phospholipids in zebrafish by DESI-MS/MS in negative and positive ion mode, respectively.[26, 46] Fish gills were mainly composed of phosphatidylcholines of *m/z* 782, *m/z* 830, *m/z* 856, *m/z* 882, *m/z* 906, *m/z* 928, *m/z* 954, *m/z* 987.[46] PCs dominate in freshwater fish gills playing important roles in structural membrane integrity and fluidity, membrane-mediated cell signaling, and cell apoptosis.[47] In contrast, in seawater fish gills mono-unsaturated phosphatidylethanolamines (PEs) are predominant. PEs in saltwater fish have been found to act as salinity regulators due to the high salt concentration of the water environment that assists in osmoregulation. It has been suggested that the absence of PEs in freshwater fish is due to the fact that fish do not undergo such an osmotic challenge in the removal of salts in a non-saline environment.[47, 48]

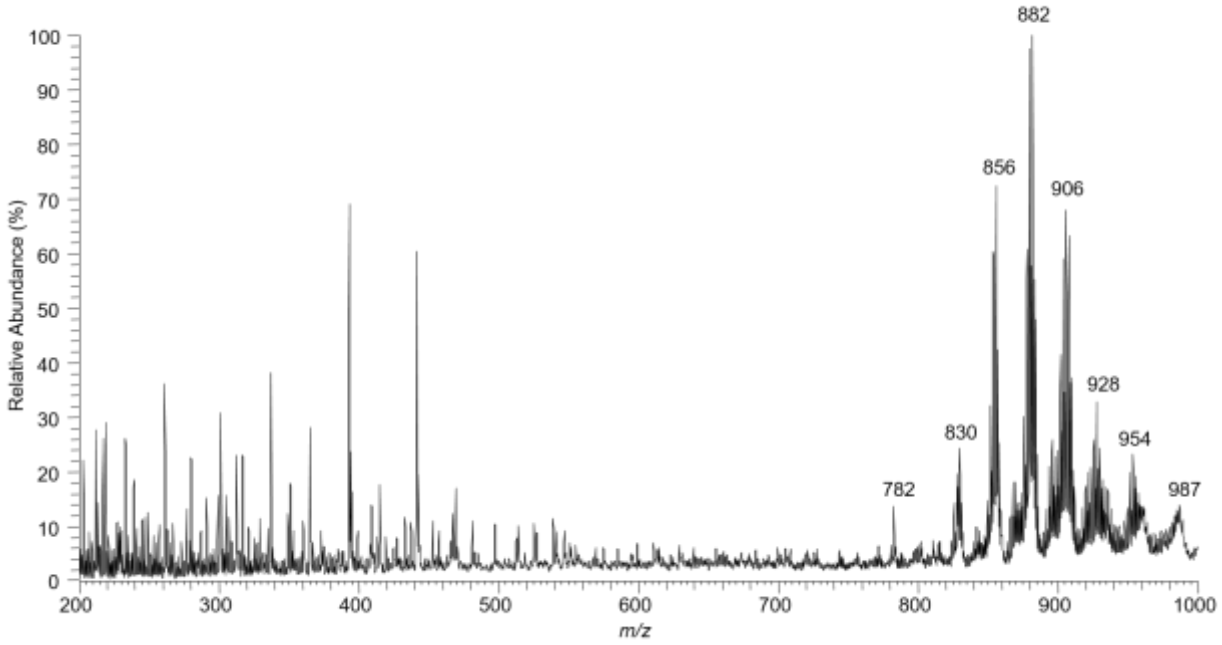

Figure 14: DESI-MS positive ion mode profile of control zebrafish gills displaying a range of phospholipids, mainly phosphatidylcholines between a mass range of *m/z* 750-1000. The most intense phospholipids from each cluster detected were *m/z* 782, *m/z* 830, *m/z* 856, *m/z* 882, *m/z* 906, *m/z* 928, *m/z* 954, and *m/z* 987.

DESI-MS/MS was performed on major peaks arising from each cluster of phospholipids in the positive ion mode. The DESI-MS/MS spectrum of phosphatidylcholines of *m/z* 782 and *m/z* 856 are shown below (Figure 15).

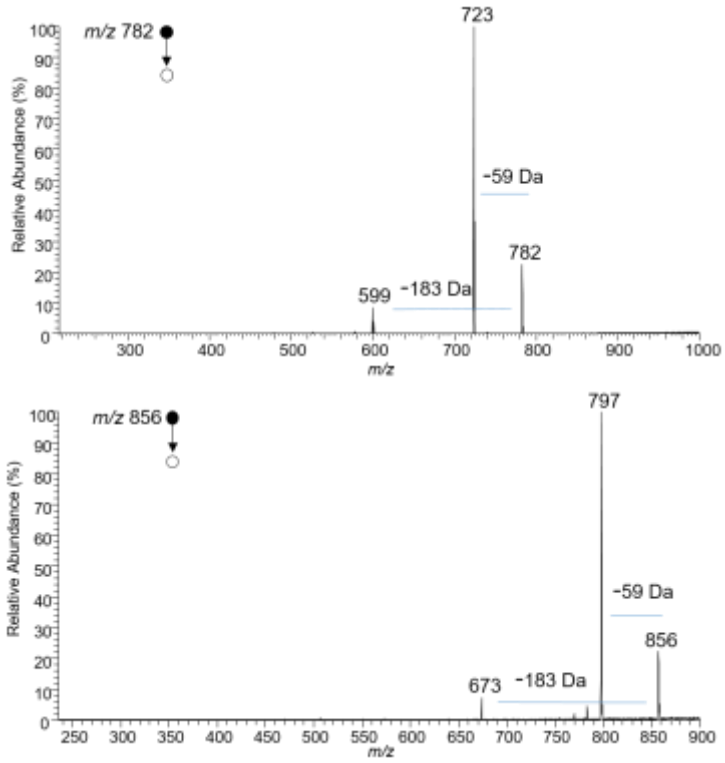

Figure 15: DESI-MS/MS spectra in positive ion mode of two phosphatidylcholines of *m/z* 782 and *m/z* 856 in control zebrafish gills.

Phosphatidylcholines of *m/z* 782 and *m/z* 856 displayed similar DESI-MS/MS fragmentation pattern. The most abundant loss was of trimethylamine, $(CH_3)_3N$ of 59 Da, minor fragments of *m/z* 599 and 673 were evident as the neutral loss of 183 Da corresponding to the phosphocholine head group. The identification of these phospholipids was not investigated further. The DESI-MS spectrum of control fish gills was merely to serve as comparison with the gill profiles from fish exposed to the ionic liquid.

The workflow involved starting from the fish exposure study of AMMOENG 130 up to mapping the ionic liquid in zebrafish tissue by DESI-MSI is shown below in Figure 16.

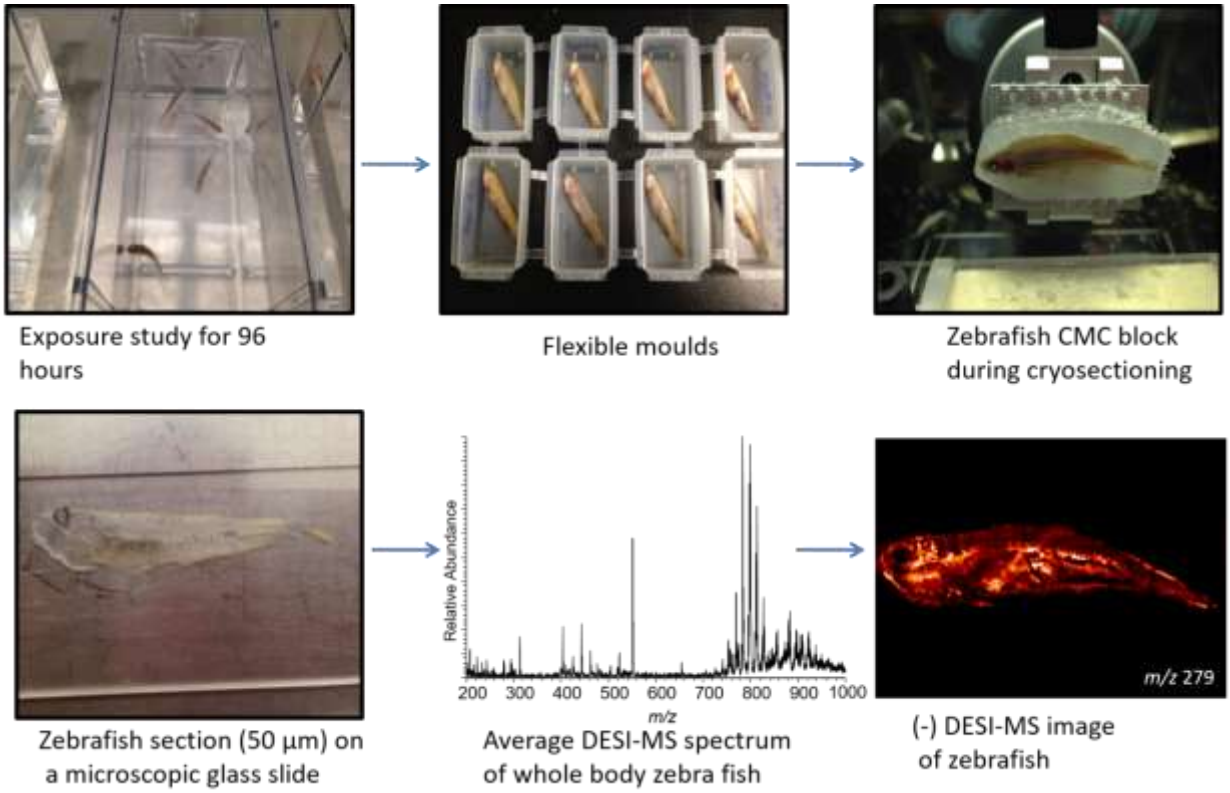

Figure 16: The workflow of whole body zebrafish tissue analysis by DESI-MS. a) Zebrafish were exposed to three concentrations of the AMMOENG 130 (1.25-5.0 mg/L) and a control run in parallel. The image displayed of deceased zebrafish is in the tank of 1.25 mg/L of AMMOENG 130. b) The fish were euthanized with MS-222, and placed in flexible moulds with CMC solution. c) Zebrafish moulds were cryosectioned and sections of 50 µm were placed onto microscopic glass slides. d) Zebrafish tissue on a microscopic slide. e) DESI-MS data of fish tissue was collected. f) DESI-MS ion images of the IL in the fish tissue were mapped for its distribution. The zebrafish image displayed is of linoleic acid $[M-H]^-$ of *m/z* 279 in control whole body zebrafish of DESI-MSI in negative ion mode.

Once DESI-MS profiles were acquired from control zebrafish gills, zebrafish gills exposed to AMMOENG 130 were analyzed for comparison. Zebrafish gill profiles exposed to concentrations of 1.25, 2.5 and 5.0 mg/L of AMMOENG 130 were collected via DESI-MS analysis (Figure 17).

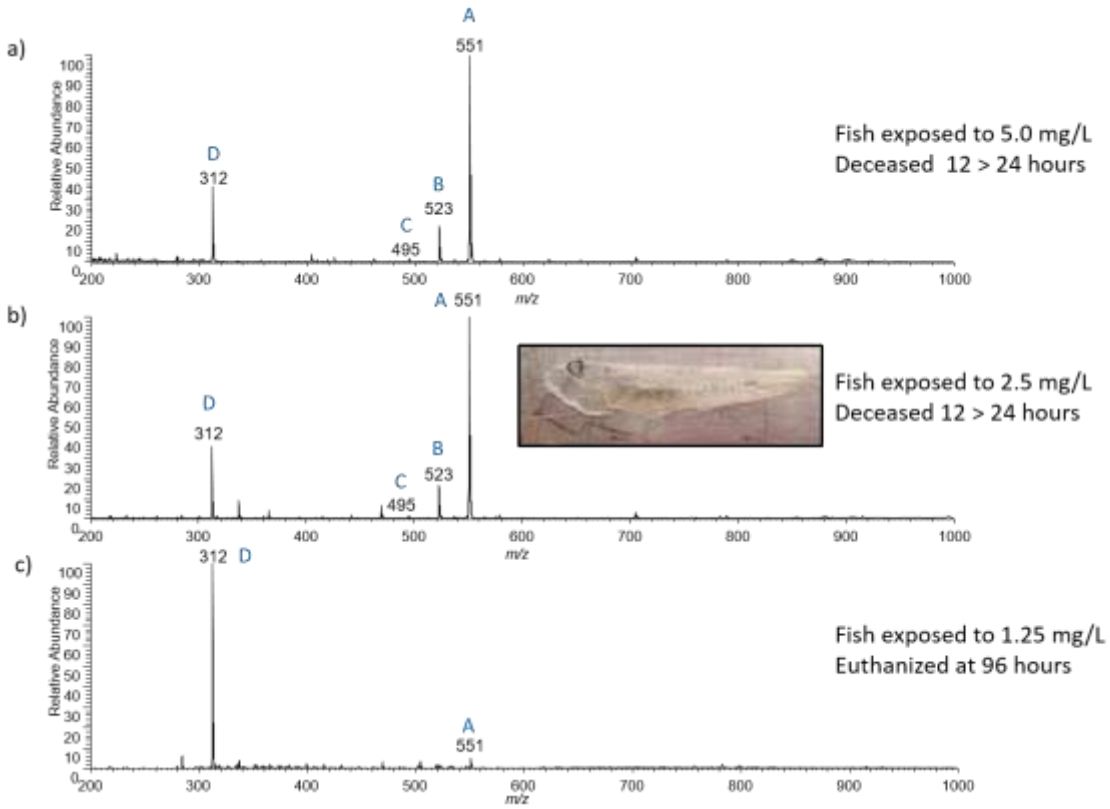

Figure 17: DESI-MS analysis in positive ion mode directly from zebrafish gills from AMMOENG 130 exposure. a) Fish exposed to 5.0 mg/L. b) Fish exposed to 2.5 mg/L. The inset image shows the zebrafish tissue on a microscopic glass slide for DESI-MS analysis. c) Fish exposed to 1.25 mg/L.

The high abundance of the IL in the gills lead to ion suppression of the naturally occurring phospholipids between the mass range of *m/z* 750-1000 (Figure 17a-c). Zebrafish gill profiles in concentrations from 1.25-5.0 mg/L demonstrated marked changes in IL abundance. AMMOENG 130 (*m/z* 551) was present in all concentrations of exposure. Interestingly, the ion of *m/z* 312 increased significantly to approximately 40% abundance at exposure concentrations of 2.5 and 5.0 mg/L (Figure 17a,b). The absence of hexadecylstearyldimethylammonium ion (*m/z* 523) and tetradecylstearyldimethylammonium/dihexadecyldimethylammonium *(m/z* 495) ions was found in fish gills from the lowest exposure concentration (Figure 17c). The major contributor in the fish gills at the lowest concentration of exposure was the ion of *m/z* 312. The major decrease in the abundance of AMMOENG 130 and the increase of the ion of *m/z* 312 lead us to speculate two

plausible outcomes, either (1) AMMOENG 130 degradation was taking place in the water during the course of the exposure study or (2) AMMOENG 130 was transformed into a metabolite for chemical elimination of the IL from the fish body.

3.4. AMMOENG 130 Degradation and Metabolism

IL chemical degradation and biodegradation pathways by microbial breakdown have been investigated with modest success. Thus far, the greatest chemical degradation efficiency for imidazolium ILs was achieved in combination of UV light and oxidative catalysts of hydrogen peroxide and titanium dioxide in which 99% was degraded after 3 days. In contrast, microbial IL degradation seems far more feasible by incorporating biodegradable ester and amide side chains enabling these functional groups to microbial enzymatic attack to improve biodegradability.[34, 37, 49] Considering the stringent conditions and specific polar functionalities to promote IL degradation, degradation was not expected under ambient conditions and a short degradation time. Nevertheless, an IL degradation study with a similar approach to that of closed bottle tests was performed to monitor the production of AMMOENG 130 degradation products.[37] Instead of monitoring the decrease in molecular oxygen content of the vessel from microbial biodegradability; AMMOENG 130 was sampled by ESI-MS by dissolving the IL in water in concentrations of 1.25, 2.5 and 5.0 mg/L to mimic IL exposure to the zebrafish. The IL was monitored for 96 hours, yet only data from time periods of 0 and 96 hours are reported for each concentration below (Figure 18).

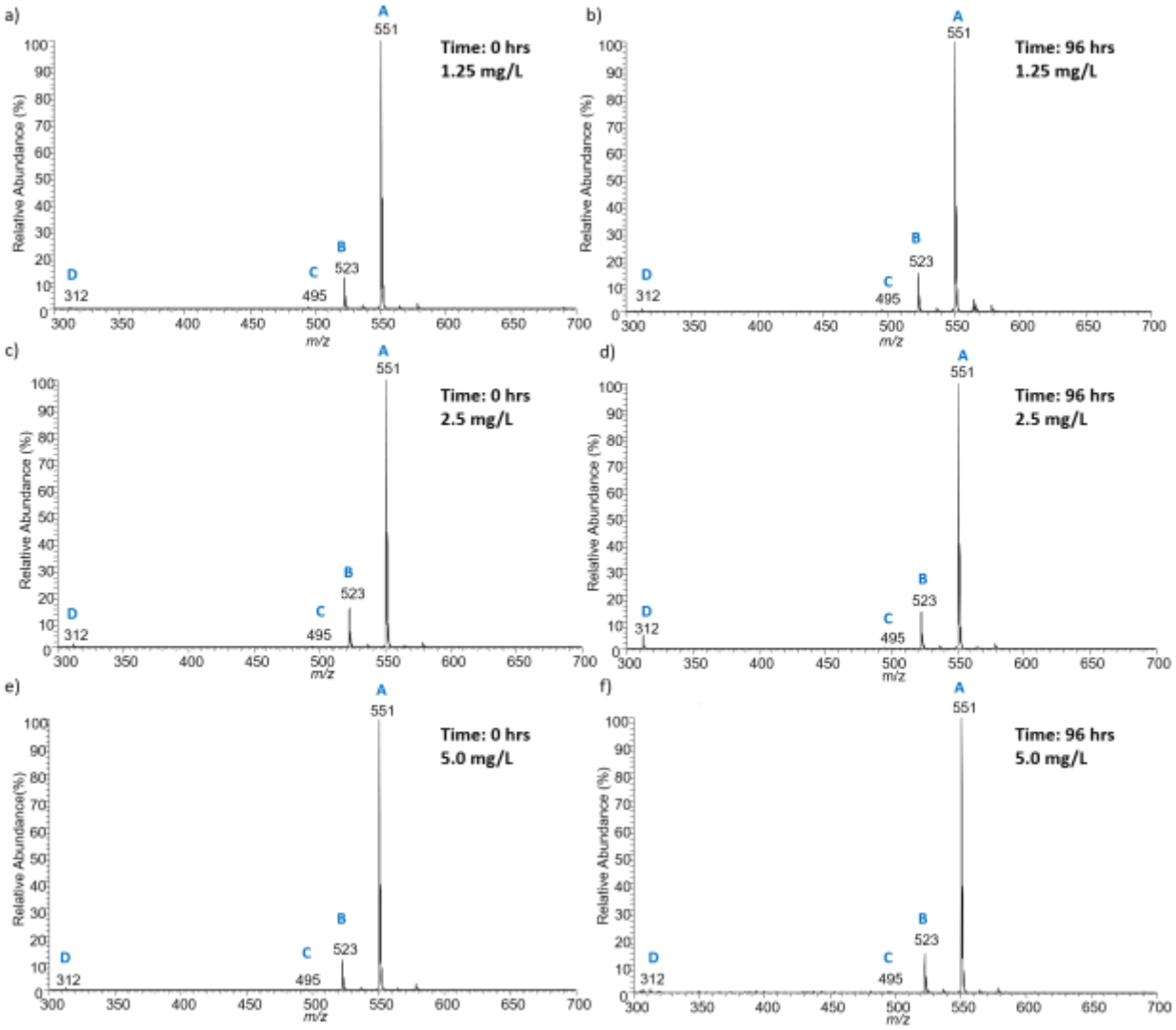

Figure 18: ESI-MS profiles of AMMOENG 130 degradation in water for a total of 96 hours, IL ions of *m/z* 551, 523, 495 and 312 were detected. a) Profile of AMMOENG 130 at 0 hrs in a 1.25 mg/L solution. b) 1.25 mg/L at 96 hrs. c) AMMOENG 130 at 0 hrs in a 2.5 mg/L solution d) 2.5 mg/L at 96 hours e) AMMOENG 130 at 0 hrs in a 5.0 mg/L solution f) 5.0 mg/L at 96 hrs.

As expected, degradation products were not encountered by MS analysis regardless of the IL concentration and exposure time. The intensity of all AMMOENG 130 ions, most importantly of *m/z* 312, remained relatively constant. Slight fluctuations of the relative abundance of the ion of *m/z* 312 were within 1-3% which can be explained by the changes encountered upon sampling different regions of the water and slight instrument variability. The MS spectra of time intervals between 0 to 96 hours for AMMOENG 130 at a concentration of 1.25 mg/L can be found in

Appendix B. AMMOENG 130 degradation in water was initially predicted to be highly unlikely; since structurally, AMMOENG 130 consists of a dimethylated quaternary ammonium head group with two unfunctionalized, saturated $C_{18}H_{37}$ alkyl chains. The sole presence of water was not sufficient to cause oxidative cleavage to produce degradation products. Degradation mechanisms require the presence of enzymatic or highly nucleophilic species to breakdown lipophilic ILs.[37] Quaternary ammonium ILs prone to degradation are composed of functionalized cation head groups requiring high temperatures and long periods of time for degradation to occur.[50]

The metabolism of xenobiotics occurs as a means of detoxification and chemical elimination with the primary function of converting the parent compound into increasingly more hydrophilic compounds for excretion. Phase I metabolism (N-dealkylation, N-demethylation, N-oxidation,) and phase II metabolism (sulfation and glucuronidation) are common enzymatic metabolic processes that are controlled by a range of Cytochrome P_{450} (CYP) families and subfamilies in zebrafish.[51, 52] In this case, the metabolic conversion of AMMOENG 130 into the metabolite may originate from dealkylation of the loss of $C_{17}H_{34.}$ Metabolic reactions involving dealkylations are a major pathway in all organisms. In fish and mammals, trifluralin accumulates extensively and a large fraction is converted into metabolites. Trifluralin's major metabolic route consists of the oxidation of one of the N-propyl side groups followed by dealkylation. Among trifluralin metabolites, a broad range of biotransformations occurs such as N-oxidations, N-dealkylations, nitro reductions and conjugations with amino acids.[53] Although, other AMMOENG 130 metabolites were not detected in this study; lipophilic ILs are known to be highly unsusceptible to metabolic biotransformation and tend to persistent relatively intact within organisms.[43] The toxicity, bioaccumulative potential and non-readily degradable characteristics of AMMOENG 130 suggests that environmental concerns in regards to incorporating these types of compounds in PCPs are not overstated.

The metabolite was characterized from zebrafish gill extract by ESI-MS and ESI-MS/MS through HRMS analysis using an LTQ-Orbitrap mass spectrometer. The metabolite was identified as stearyltrimethylammonium ion, $[C_{21}H_{46}N]^+$. The accurate mass detected was 312.3619 Da and

the calculated exact mass as 312.3632 Da with a mass error of 4.2 ppm (Figure 19a). AMMOENG 130 was present in the zebrafish gill extract (*m/z* 550.6267) with a mass error of 4.4 ppm. The major fragment of the metabolite was the ion of *m/z* 296.3303 (Figure 19b), a common fragment with the parent molecule AMMOENG 130. The exact mass of the fragment was calculated to 296.3317 Da corresponding to a mass error of 4.7 ppm.

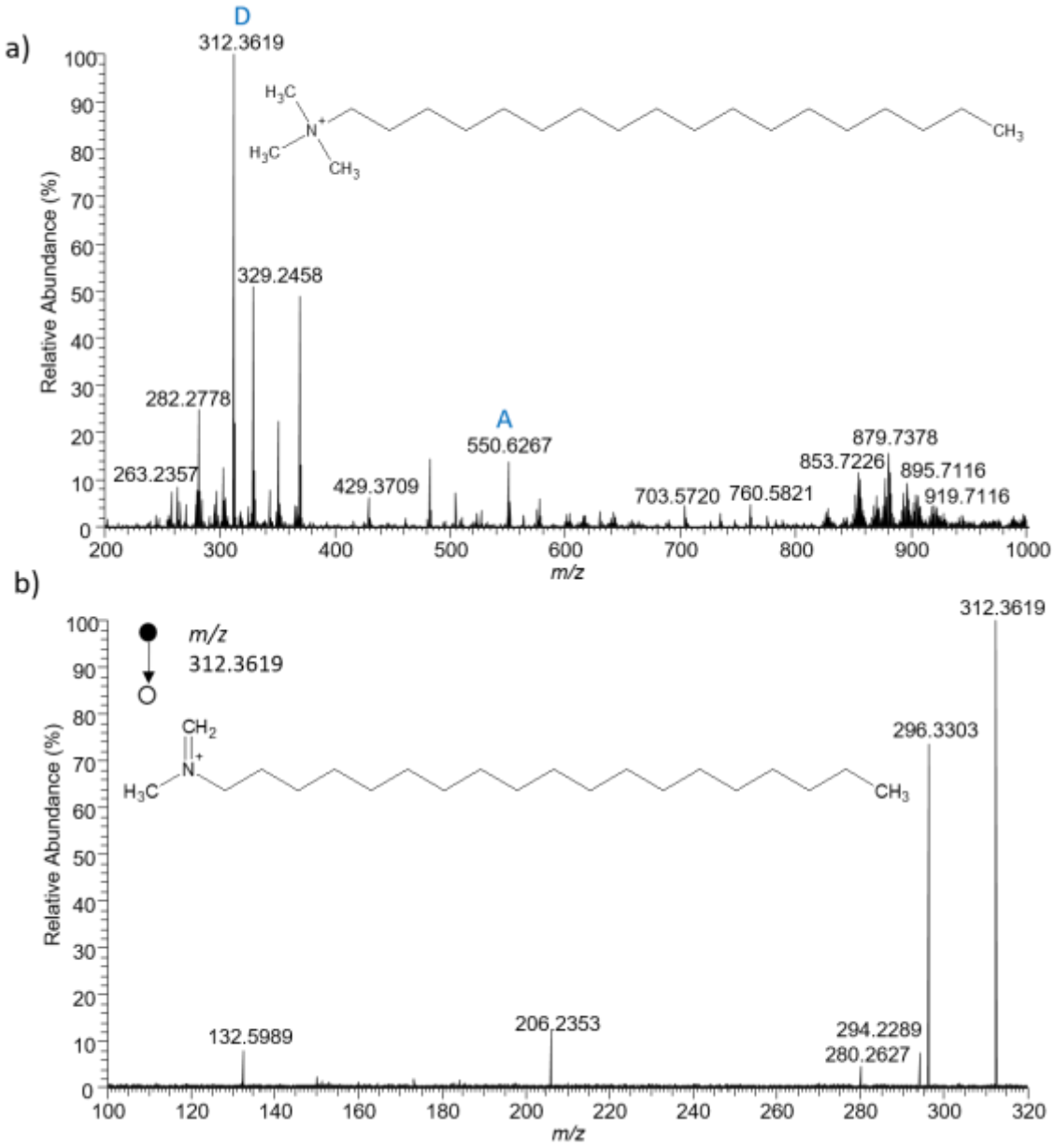

Figure 19: Metabolite characterization from zebrafish gill extract prepared from fish exposed to 1.25 mg/L of AMMOENG 130 by HRMS analysis with a LTQ-Orbitrap mass spectrometer. a) Full scan ESI-MS spectrum of the gill extract. AMMOENG 130 of *m/z* 550.6267 and the metabolite of *m/z* 312.3619. b) ESI-MS/MS of the metabolite using a collision energy between 50-51%. The

inset tentative molecular structure is of $[C_{20}H_{42}N]^+$ corresponding to the fragment of *m/z* 296.3303. Unknown fragments of *m/z* 294.2289, *m/z* 280.2627, *m/z* 206.2353 and *m/z* 132.5983 were also detected.

In regards to these findings, we propose that the zebrafish actively metabolized AMMOENG 130 during the course of exposure into a more polar compound for elimination and to reduce the IL's persistence and toxicity.

3.5. Elucidation of AMMOENG 130 Accumulation in Zebrafish

DESI-MS imaging was used to localize the accumulation of AMMOENG 130 in zebrafish tissue in all concentrations of exposure. Tissues were collected and analyzed from varying depths of the fish body, yet sections closer to the center of the fish body containing most biological systems simultaneously such as brain, gill and organs were mapped for AMMOENG 130.

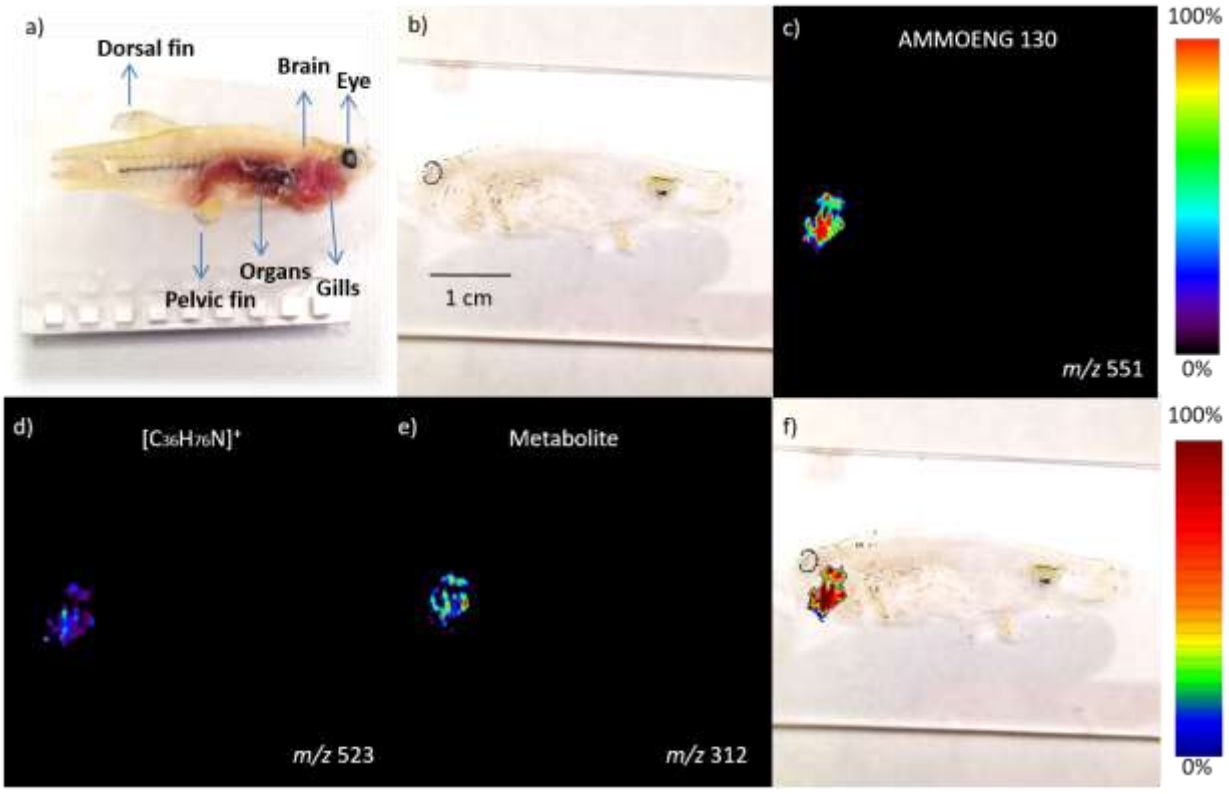

Figure 20: Accumulation of AMMOENG 130 in whole body zebrafish exposed to concentrations of 5.0 mg/L by DESI-MS imaging a) Zebrafish during crysosectioning. b) Optical image of the zebrafish tissue section. c) Accumulation of AMMOENG 130 molecular ion of *m/z* 551. d) Accumulation of the IL ion of *m/z* 523. e) Accumulation of the metabolite of *m/z* 312. f) Overlay

of the optical image with the DESI-MS image of AMMOENG 130. All images and overlays produced in both scale bars were normalized in Biomap.

In fish exposed to IL concentrations of 5.0 mg/L, AMMOENG 130, hexadecylstearyldimethylammonium, and the metabolite accumulated in the gills (Figure 20). Zebrafish gills are responsible for a variety of physiological functions including respiration, excretion of nitrogenous waste, osmoregulation, ionoregulation and acid-base regulation.[54, 55] Upon physiological damage of gill lamellae, the gill surface area for respiration is decreased, the fish gas-exchange process is disrupted and no longer functional.[4] The gills are a major site of damage induced by environmental pollutants, it has been suggested as a crucial site of metabolism and for the excretion of toxins.[54] Accumulation of AMMOENG 130 in the gills and epithelia was found at a concentration of 2.5 mg/L (Figure 21). The accumulation in the outermost part of the tissue was attributed to the accumulation in fish epithelia. The complex and multifunctional epidermal barrier is capable of defending against the introduction of harmful xenobiotics however, lipophilic ILs upon insertion can cause havoc on the structural integrity of membranes, and thus accumulate. The highly toxic exposure concentrations near the LC_{50} induced mortality and did not allow the IL to accumulate in other organs during a short time of exposure of merely 24 hours.

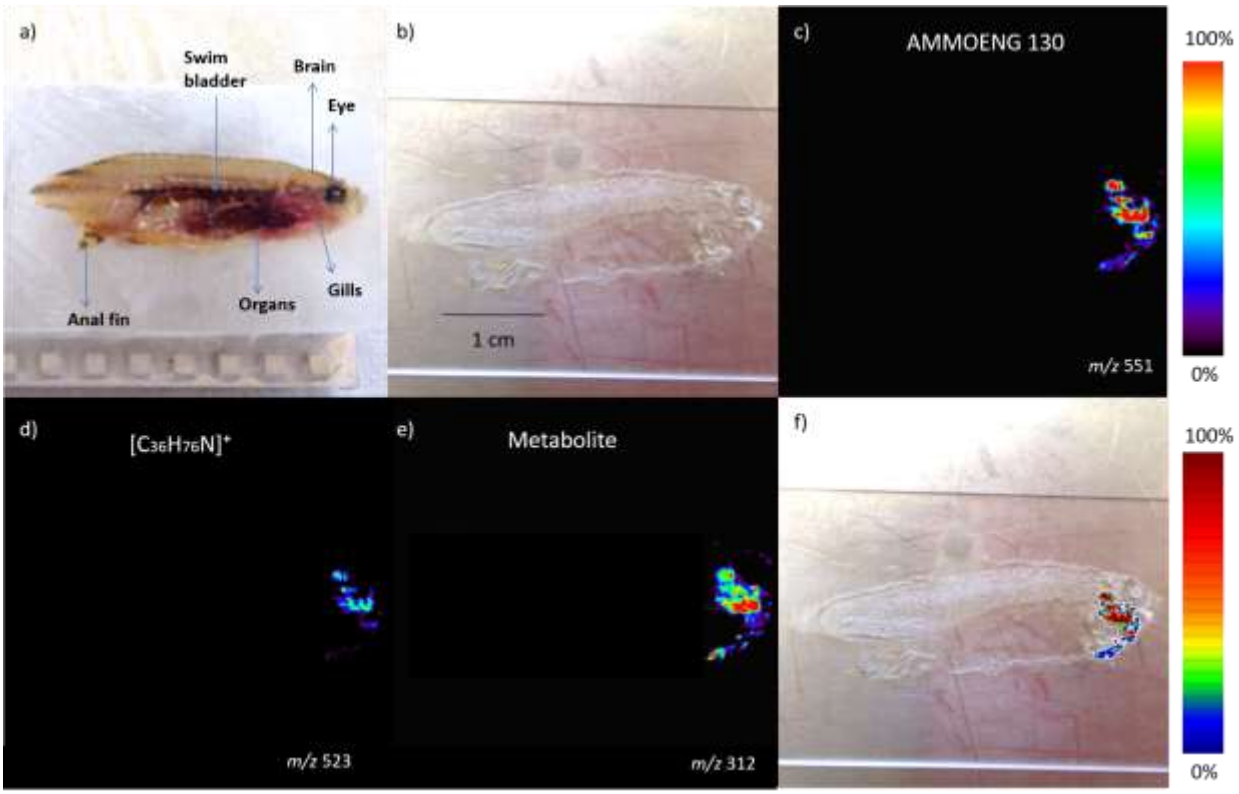

Figure 21: Accumulation of AMMOENG 130 in whole body zebrafish exposed to concentrations of 2.5 mg/L by DESI-MS imaging a) Zebrafish image of organ systems. b) Optical image of the zebrafish tissue section. c) Accumulation of AMMOENG molecular ion of *m/z* 551. d) Accumulation of the IL ion of *m/z* 523. e) Accumulation of the metabolite of *m/z* 312. f) Overlay of the tissue optical image with the DESI-MS image of AMMOENG 130. All images and overlays produced in both scale bars were normalized in Biomap.

Zebrafish was mapped for AMMOENG 130 exposed to 1.25 mg/L, however only AMMOENG 130 (*m/z* 551) and the metabolite (*m/z* 312) were detected (Figure 22). The regions of accumulation in a lower concentration differed from concentrations of 5.0 and 2.5 mg/L due to a longer exposure time of 96 hours.

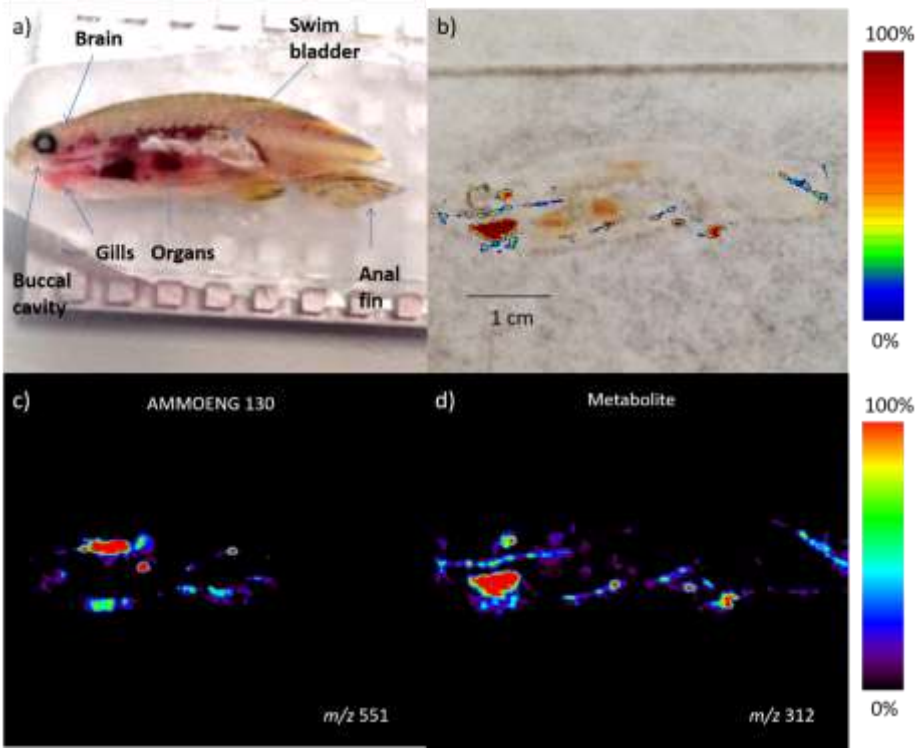

Figure 22: Accumulation of AMMOENG 130 analyzed by DESI-MS imaging in whole body zebrafish exposed to a concentration of 1.25 mg/L. a) Optical image of CMC embedded fish during cryosectioning outlining organ systems. b) Optical image of the zebrafish tissue section under analysis overlapped with the DESI-MS image of the metabolite. Images were normalized in both scale bars with Biomap. c) Accumulation of AMMOENG 130 (*m/z* 551). d) Metabolite accumulation (*m/z* 312).

The IL was primarily localized in the respiratory and nervous system of the zebrafish. AMMOENG 130 was distributed in the brain, gills, and other unidentified regions (Figure 22c); while the metabolite was mainly present in high abundance in the gills and in lower abundance in the brain (Figure 22d). Both, the IL and the metabolite showed an accumulation pattern in membrane-rich areas. AMMOENG 130 was found in highest abundance in the brain suggesting that the IL was capable of penetrating the blood brain barrier (BBB), the brain's main defense system against toxic substances with subsequent accumulation in the nervous system. Lipophilic ILs, like AMMOENG 130 resemble endogenous lipids in membranes; the amphiphilic nature of these species containing a positively charged hydrophilic head group and long hydrophobic alkyl chains allows for membrane insertion. Yet, to ultimately breach the brain via the BBB highly depends on the size of the xenobiotics in question. The zebrafish BBB is a highly selective size dependent barrier that allows the passive diffusion of lipid-soluble molecules across the membrane with

greater ease than hydrophilic molecules.[56] Therefore, AMMOENG 130 most likely has greater ease than the metabolite of diffusing through the BBB as demonstrated within the images that AMMOENG 130 accumulation in the brain was more intense and distributed in more brain tissue than the metabolite as shown in Figure 22c.

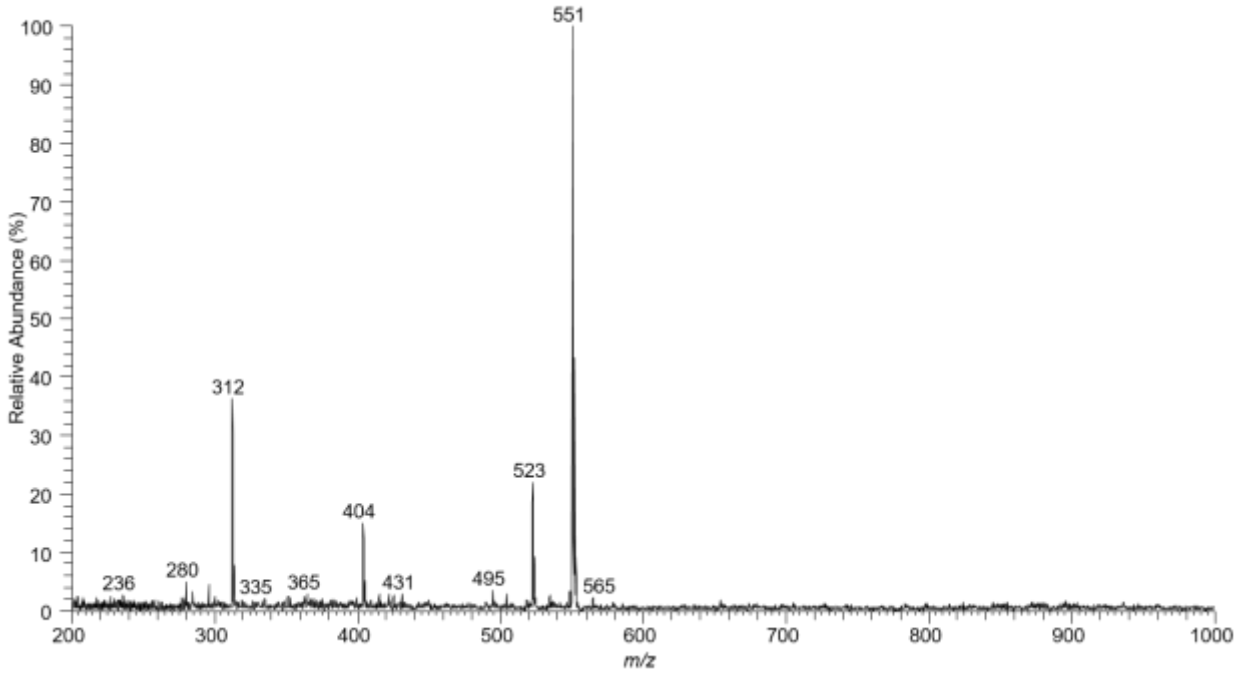

Figure 23: DESI-MS spectrum of a selected part of the zebrafish brain containing AMMOENG 130 and the metabolite.

A part of the zebrafish brain was selected and the DESI-MS spectrum is shown in Figure 23. The intensity of AMMOENG 130 compared to the metabolite is greater in the brain. The AMMOENG 130 peak of *m/z* 551 and the metabolite peak of *m/z* 312 were individually selected to obtain an image of the distribution of the ion. With respect to metabolism, we can only speculate that biotransformation occurred in fish gills and the metabolite either partly diffused from gills into the brain and/or AMMOENG 130 was metabolically transformed locally in the brain to give rise to the metabolite. In either case, both plausible metabolic pathways indicate that the metabolism of AMMOENG 130 in two major organ systems: the respiratory and nervous system. The higher

abundance of metabolite in the gill tissue leads us to suggest that gills play a major role in the metabolic biotransformation of AMMOENG 130. Accumulation of AMMOENG-type ILs in the nervous system is concerning in regards to respiratory toxicity and neurotoxicity. The metabolite consists of a trimethylated ammonium head group with a $C_{18}H_{37}$ hydrophobic alkyl chain, the cation moiety structurally resembles biological neurotransmitters choline and acetylcholine in the brain. Choline transport through the blood brain barrier is carrier mediated, saturable and the uptake of nitrogen-methylated choline analogs can block choline binding active sites causing inhibition. Quaternary ammonium binding recognition is a major transport restraint in the BBB, a pyrene derivative, 2-[-4-(1-pyreny l-butyryloxy-ethyl)]-trimethylammonium ion has been shown to be a choline competitive inhibitor with a 20-fold increase in affinity compared to choline in rat synaptosomes.[57] The increased affinity was a result of the hydrophobicity of the compound interacting with the membrane core or adjacent hydrophobic binding regions. Subsequently, AMMOENG 130 and the metabolite may act as an inhibitor, effectively entering the BBB, accumulating in the brain causing neurotoxic effects. These findings are rather concerning since AMMOENG type ILs may potentially be neurotoxins for zebrafish. Nevertheless, AMMOENG 130 and its metabolite's neurotoxicity must be investigated further to come to conclusive results.

Although, the accumulation of AMMOENG 130 was not detected in the liver, pancreas or gastrointestinal system by DESI-MS analysis; the conversion of AMMOENG 130 to the metabolite may originate as a means of extrahepatic metabolism. Zebrafish Cytochrome P450 2J (CPY2J) subfamilies have been identified as catalysts for arachidonic acid metabolism in extrahepatic tissues of many species including the zebrafish with high degree of similarity to the activity of CPY2J2 enzyme in humans.[58] Spot fish (*Leiostoma xanthrus)* exposed to radiactive tributyltin (^{14}C-TBT) in the water metabolized ^{14}C-TBT into dibutyltin, monobutyltin, and other ^{14}C-TBT conjugates in extrahepatic tissues. TBT concentrations monitored after 2 and 4 days remained considerably higher in gill tissue compared to liver, brain and muscle tissue. The metabolism, degradation and environmental impact of the AMMOENG series ILs are still not well understood

and to date have not been thoroughly explored. Therefore, this research can serve as a starting point to study AMMOENG based ILs.

3.6. DESI-MSI as a Potential Tool for Monitoring Environmental Pollutants

The suitability of DESI-MSI as a potential monitoring technique was explored to asses if environmentally relevant IL concentrations of exposed aquatic organisms could be evaluated by this technique. DESI-MS quantitative analysis of common pharmaceutical compounds has been previously evaluated by Ifa et al. by assessing the performance of surfaces such as PMMA, flat, printed glass and porous PTFE surfaces.[5] Porous PTFE surfaces provided the best performance in terms of sensitivity and minimizing carry over. Quantitative analysis was carried out in porous PTFE surfaces to measure analytical parameters including the linearity, S/N, LODs, LOQs, inter-day and intra-day precision of propranolol using an isotopically labeled internal standard, propranolol-d_7 and a propranolol analog, atenolol. Porous PTFE's enhanced performance was due to the weak sample-surface interactions such that desorption of the analyte is favoured. The porous surface avoids the analyte of interest from being removed too quickly from the surface, creating a stable signal, stable intensity and at the same time minimizing carryover from adjacent spots.[5]

A study to evaluate the limit of detection of AMMOENG 130 was performed by DESI-MS analysis. A range of AMMOENG 130 concentrations were spotted onto PTFE coated microscopic glass slides with a spot volume of 1 µL. AMMOENG 130 concentrations of 1 ng/L, 10 ng/L, 100 ng/L, 1 µg/L were spotted onto PTFE coated microscopic glass slides and DESI-MS spectra was collected for two minutes, yet the AMMOENG 130 signal of *m/z* 551 was not detected from the average noise level. Subsequently, concentrations of 10 µg/L, 100 µg/L, 1 mg/L, 10 mg/L and 100 mg/L were spotted onto a PTFE coated microscopic glass slide (Figure 23).

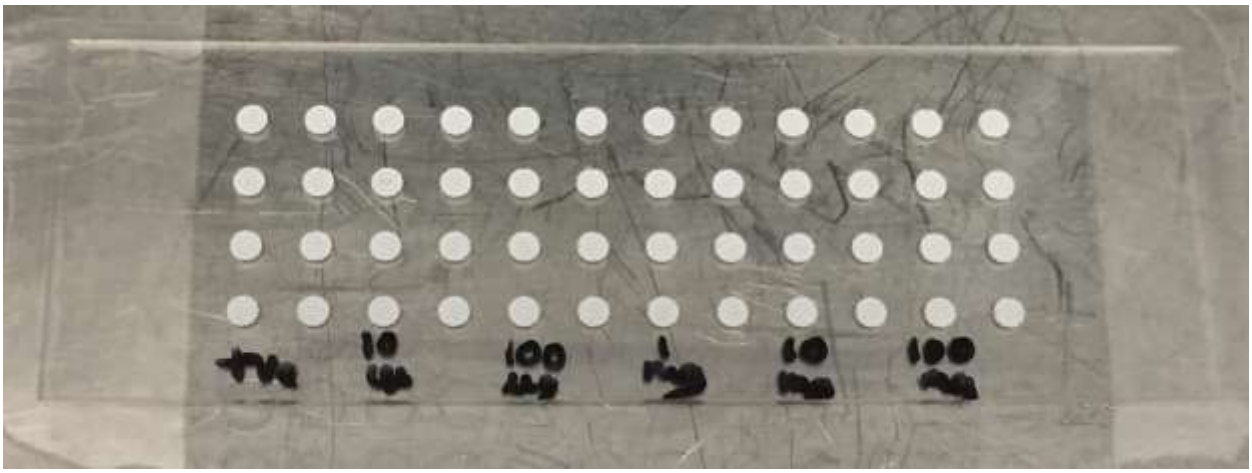

Figure 24: Optical image of the 1 µL AMMOENG 130 spots onto a PTFE coated microscopic glass from concentrations of 10 µg/L, 100 µg/L, 1 mg/L, 10 mg/L and 100 mg/L from left to right.

The limit of detection was determined as the lowest concentration of AMMOENG 130 that could be detected by DESI-MS analysis. The LOD was measured by spotting known concentrations and evaluating if the AMMOENG 130 signal to noise (S/N) ratio was 3 times greater. Experimentally, the average S/N fluctuation was calculated from an average full scan collected for two minutes and compared to the AMMOENG 130 signal of *m/z* 551. The DESI-MS spectrum for all the AMMOENG 130 concentrations tested is shown below in Figure 24.

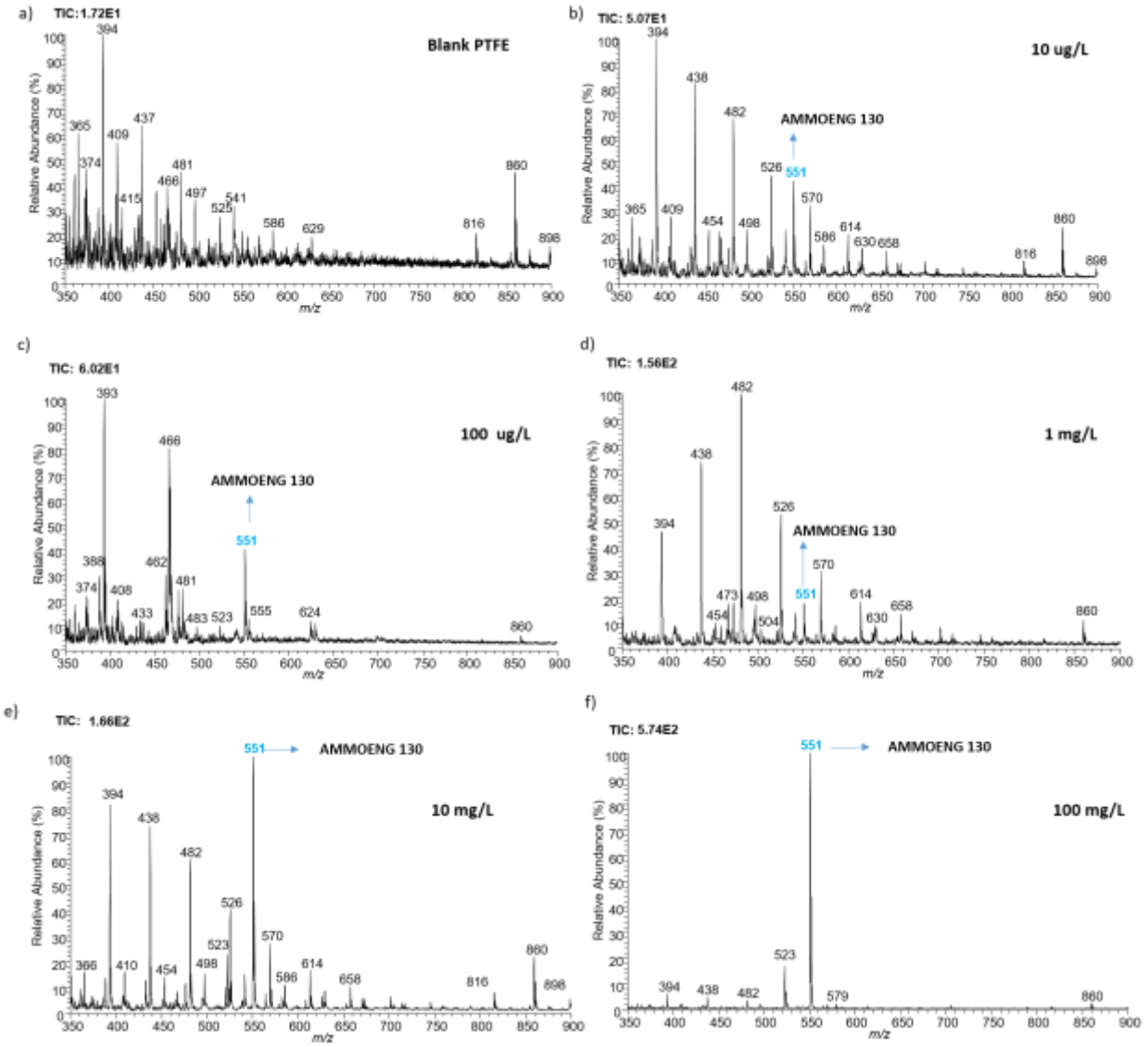

Figure 25: DESI-MS analysis to assess the limit of detection of AMMOENG 130 from concentrations between 10 µg/L to 100 mg/L from an average full scan spectrum collected for a total of 2 minutes. a) DESI-MS spectrum of blank PTFE b) AMMOENG 130 concentration of 10 µg/L. c) AMMOENG 130 concentration of 100 µg/L. d) AMMOENG 130 concentration of 1 mg/L. e) AMMOENG 130 concentration of 10 mg/L. f) AMMOENG 130 concentration of 100 mg/L.

For a concentration of 10 µg/L, the total ion count was 1.32 x 10^1 during a span of two minutes for data acquisition. The average noise was approximated to 14% relative abundance. The average AMMOENG 130 signal was 1.09 x 10^1 counts and a relative abundance of 82.9%. In this case, the S/N ratio is approximately 6 times greater than the noise level. Figure 25 shows a better view of the AMMOENG 130 signal in a mass range of *m/z* 450-650.

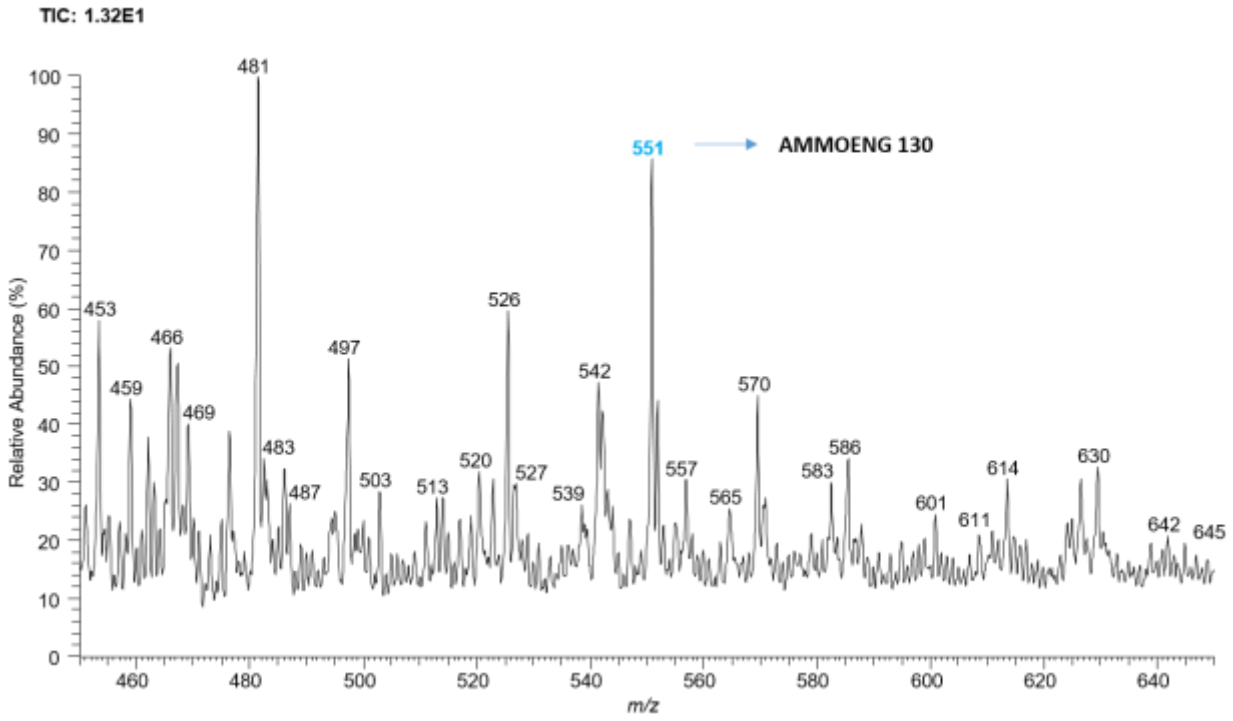

Figure 26: DESI-MS spectrum of AMMOENG 130 spotted onto PTFE coated microscopic glass slide at a concentration of 10 µg/L in a mass range of *m/z* 450-650.

A similar experiment was conducted by spotting 1 µL onto PFTE coated microscopic glass slides however, concentrations of 8, 9, 10, 11 and 12 µg/L of AMMOENG 130 were assessed (Figure 26).

Figure 27: Optical image of the 1 µL AMMOENG 130 spots onto a PTFE coated microscopic glass from concentrations of 10 µg/L, 100 µg/L, 1 mg/L, 10 mg/L and 100 mg/L from left to right.

AMMOENG 130 concentrations of 8 and 9 µg/L were not detected, the AMMOENG 130 signal of *m/z* 551 could not be distinguished from the average noise level. However, in concentrations of 10, 11 and 12 µg/L AMMOENG 130 was detected between 3-5 times higher than the average noise level. The limitations associated with determining the limit of detection with this surface analysis technique is that the analyte may not always dry homogenously onto the surface. A "coffee ring effect" arises from depositing an aliquot of the analyte onto the surface and allowing the sample to air dry. Depending on the surface type, a higher deposition of the analyte can be observed in the outer rims of the spot. Rough or porous surfaces (i.e. PTFE) show better signal stability and reproducibility than smooth ones preventing a "washing effect" and "coffee ring effect".[59] These phenomena, without a doubt, can compromise the analytical performance and reproducibility of the DESI measurements.

Ifa et al. determined the lowest concentration detected by DESI-MS analysis from 9 commonly used drugs such as verapamil, dobutamine and diazepam in positive ion mode and 3 compounds (chloramphenicol, ibuprofen and PG(16:0/18:0)) in negative ion mode.[5]

Table 1. Lowest concentrations detected for representative compounds on different surfaces

Compound	Polarity	Collision energy	Precursor → product (*m/z*)	Lowest conc. detected (ng/µL)			
				PMMA	PTFE-printed	Porous PTFE	PTFE sheets
(1) Propranolol	+	27	*260.2* $[M+H]^+ \rightarrow$ *183.2*	1	0.01	0.01	0.01
(2) Testosterone	+	20	*289.3* $[M+H]^+ \rightarrow$ *253.2*	1	0.1	10	1
(3) Dobutamine	+	25	*302.3* $[M+H]^+ \rightarrow$ *137.2*	1	1	10	1
(4) Verapamil	+	23	*445.4* $[M+H]^+ \rightarrow$ *303.3*	0.1	0.1	0.01	0.1
(5) Chloramphenicol	−	27	*321.0* $[M-H]^- \rightarrow$ *257.0*	1	0.1	0.01	0.1
(6) Ibuprofen	−	20	*205.2* $[M-H]^- \rightarrow$ *161.2*	100	10	1	100
(7) Diazepam	+	30	*285.3* $[M+H]^+ \rightarrow$ *257.1*	0.1	0.01	0.01	0.01
(8) Roxithromycin	+	20	*837.7* $[M+H]^+ \rightarrow$ *679.2*	1	0.01	0.01	0.1
(9) Carbamazepine	+	25	*237.2* $[M+H]^+ \rightarrow$ *194.2*	0.1	0.01	0.01	0.1
(10) Acetylcholine	+	25	*146.3* $[M+H]^+ \rightarrow$ *87.2*	0.1	0.01	0.01	0.1
(11) PG (16:0, 18:0)	−	18	*747.4* $[M-H]^- \rightarrow$ *281.3*	100	10	1	10
(12) Angiotensin	+	20	*523.8* $[M+2H]^{+2} \rightarrow$ *784.4*	1	0.1	0.1	0.1

Figure 28: The lowest concentration detected from pharmaceutical compounds in positive and negative ion mode analyzed by DESI-MS analysis. Reprinted with permission from reference [5].

LODs from pharmaceuticals analyzed in positive ion mode ranged from 0.01-10 ng/µL while in negative ion mode LODs ranged from 0.01-100 ng/µL. When these concentrations are converted for comparison, LODs range from 10-10,000 µg/L in positive ion mode and 10-100,000 µg/L in

negative ion mode. The LOD for AMMOENG 130 was found to be either comparable with certain pharmaceutical compounds or substantially better with compounds in both polarities. The ionic nature of AMMOENG 130 contributes for increased sensitivity, and therefore a lower limit of detection. Compared with the above results, DESI-MS analysis appears suitable for monitoring contaminants at low μg/L concentrations. Using PTFE surfaces as means of determining AMMOENG 130's LOD provides an indication that environmentally relevant concentrations can be assessed. However, for quantitative analysis of accumulated ionic liquids in biological tissue of aquatic organisms the LOD, LOQ, linearity, inter-day and intra-day precision must be evaluated with an appropriate internal standard separately for the specific biological tissue type (i.e. zebrafish) under analysis, since biological matrix effects must be taken into consideration for IL recovery from matrix and for potential matrix ion suppression effects that can increase all analytical parameters. Quantitative DESI-MS analysis is still in its infancy many improvements have yet to be made to obtain highly reproducible results.[60]

3.7. Conclusion and Future Perspectives

It was the intent of this thesis to introduce DESI-MSI as a novel, rapid and sensitive technique to explore the accumulation of a toxic IL in a popular aquatic vertebrate model. DESI-MSI was capable of providing simultaneous characterization, accumulation and metabolite detection of AMMOENG 130 with minimal sample preparation and short analysis times. Although the metabolite encountered in zebrafish gills of *m/z* 312 was also found in the standard AMMOENG 130 solution, the fragmentation pattern and the HRMS experiments revealed that stearyltrimethylammonium ion was indeed the same molecule in both cases. In regards to the metabolic IL transformation, we suspect that either AMMOENG 130 was converted into the stearyltrimethylammonium ion by zebrafish or perhaps, AMMOENG 130 was partially eliminated from fish body during the exposure study and the stearyltrimethylammonium ion was accumulated from water spiked with AMMOENG 130 standard already containing stearyltrimethylammonium. It is difficult to definitively assign the cause of the accumulation and metabolism however, the latter seems to be less likely such that lipophilic, non-easily degradable

and bioaccumulative compounds can persist indefinitely in aquatic organisms, water and soil due to physical or chemical absorption/adsorption.[27, 49] Nevertheless, DESI-MSI provided new insights into the accumulation pattern of AMMOENG 130 and revealed a dealkylated metabolite in fish respiratory and nervous system. The accumulation of the IL and the metabolite in the nervous system leads us to further question whether this compound could illicit neurotoxic effects and potentially act as a neurotoxin to zebrafish. In the environment, IL persistence within aquatic organisms can lead to indirect toxic effects by secondary poisoning in ecosystems and negatively impact wildlife in the long term, therefore more research still needs to be conducted on AMMOENG based ILs. The potential for quantitative IL monitoring with DESI-MSI has been demonstrated here by determining the limit of detection for AMMOENG 130. The application of this technique may be extended to bioaccumulation studies involving IL exposure of environmentally relevant concentrations in zebrafish and other small aquatic organisms. Hence, this research may open new avenues in the study of ecotoxicology of small aquatic organisms from environmental exposure of not only ionic liquids but of a wide range of chemical pollutants, pesticides and drugs to monitor their accumulation, persistence, degradation and metabolism simultaneously.

Chapter IV

Publications

In this chapter, I have included all works in which I have participated in during my time as a Master student that resulted in publications. I have outlined my specific contributions for each work. Due to copyright reasons the publications are available online with the provided DOI.

1. Publication #1: Monitoring toxic ionic liquids in zebrafish (*Danio rerio*) via desorption electrospray ionization mass spectrometry imaging (DESI-MSI)

Authors: Consuelo J. Perez, Alessandra Tata, Michel L. De Campos, Chun Peng, and Demian R. Ifa.

Journal: Journal of the American Society for Mass Spectrometry (Submitted)

Contributions: My contributions in this publication were performing all of the experiments, data analysis and interpretation, created all of the figures and tables in the manuscript and the supporting information. Edited and reviewed the manuscript for submission to the Journal.

2. Publication #2: Imprint DESI-MSI monitors secondary metabolite production during antagonistic fungi interaction.

Authors: Alessandra Tata, Consuelo J. Perez, Mark L. Bayfield, Mark N. Eberlin, and Demian R. Ifa.

Journal: Analytical Chemistry, Volume 87, Issue 24, Pages 12298-12305. 2015.

DOI: 10.1021/acs.analchem.5b03614

Contributions: My contributions involved participating in all of the laboratory experiments except for the HPLC-MS experiments on the LTQ-Orbitrap, partial involvement in the data analysis and interpretation. Created some figures for the manuscript and supporting information. Reviewed and edited the manuscript before submission to Analytical Chemistry.

Abstract

Direct analysis of microbial cocultures grown on agar media by desorption electrospray ionization mass spectrometry (DESI-MS) is quite challenging. Due to the high gas pressure upon impact with the surface, the desorption mechanism does not allow direct imaging of soft and irregular surfaces. The divots in the agar, created by the high-pressure gas and spray, dramatically change the geometry of the system decreasing the intensity of the signal. In order to overcome this limitation, an imprinting step, in which the chemicals are initially transferred to the flat hard surfaces, was coupled to DESI-MS and applied for the first time to fungal cocultures. Note that fungal cocultures are often disadvantageous in direct imaging mass spectrometry. Agar plates of fungi present in complex topography due to the simultaneous presence of dynamic mycelia and spores. One of the most devastating diseases of cocoa trees is caused by fungal phytopathogen *Moniliophthora roreri*. Strategies for pest management include the application of endophytic fungi, such as *Trichoderma harzianum*, that act as biocontrol agents by antagonizing *M.roreri*. However, the complex chemical communication underlying the basis for this phytopathogen-dependant biocontrol is still unknown. In this study, we investigated the metabolic exchange that takes place during the antagonistic interaction between *M.roreri* and *T. harzianum*. Using imprint-DESI-MS imaging we annotated the secondary metabolites released when *T. harzianum* and *M. roreri* were cultured in isolation and compared these to those produced after three weeks of coculture. We identified and localized four phytopathogen-dependant secondary metabolites, including T39 butenolide, harzianolide, and sorbicillinol. In order to verify the reliability of the imprint-DESI-MS imaging data and evaluate the capability of tape imprints to extract fungal metabolites while maintaining their localization, six representative plugs along the entire *M.roreri*/*T.harzianum* coculture plate were removed, weighed, extracted, and analyzed by liquid chromatography-high resolution mass spectrometry (LC-HRMS). Our results not only provide a better understanding of *M.roreri*-dependant metabolic induction in *T.harzianum*, but may seed novel directions for the advancement of phytopathogen-dependant biocontrol, including the generation of optimized *Trichoderma* strains against *M.roreri*, new biopesticides, and fertilizers.

3. Publication #3: Evaluation of imprint DESI-MS substrates for the analysis of fungal metabolites.

Authors: Alessandra Tata, Consuelo J. Perez, Moriam Ore, Dragos Lostun, Sylvie Morin, and Demian R. Ifa.

Journal: Royal Society of Chemistry Advances, Volume 5, Pages 75458-64. 2015.

DOI: 10.1039/C5RA12805F

Contributions: My contributions to this publication included participating in all of the laboratory experiments. Partial contributions in regards to figures for the manuscript and supporting information. Reviewed and edited the manuscript before submission to Royal Society of Chemistry Advances.

Abstract

Mass spectrometry (MS) has become an important tool in microbiology for the identification of microorganisms and for monitoring the production of microbial secondary metabolites. Therefore, several ambient mass spectrometry techniques have been applied in the last few years. Although desorption electrospray ionization mass spectrometry (DESI-MS) is the most popular ambient MS technique, its application in the direct analysis of fungal compounds is still not well established. The irregular or uneven nature of the colony, the absorbent properties of the growth medium and the need for a firm surface for effective ionization hinder the direct screening of metabolites in fungal cultures by DESI-MS analysis. To overcome these limitations, in this study, we tested different surfaces, such as tape, porous polytetrafluoroethylene (PTFE), thin layer chromatography (TLC) surfaces, filter paper, flat silicon wafers and porous silicon (pSi), to obtain the best imprint-DESI-MS outcome with fungal cultures of *Trichoderma harzianum* for metabolite screening. We also evaluated the efficiency of the surfaces for the DESI-MS of small polar fungal metabolites in regard to signal intensity, signal stability and imaging suitability. The silicon surfaces provided the highest signal intensity for the fungal metabolites. PTFE and filter paper demonstrated relatively high signal stabilities that could be useful for prolonged DESI-MS/MS experiments, whereas tape was found to be the best option for DESI-MS imaging. The

imprint on a tape surface was the only one capable of maintaining the structural features of the concentric conidial rings of *T. harzianum*.

4. Publication #4: Reactive DESI-MS imaging of biological tissues with dicationic ion-pairing compounds.

Authors: Dragos Lostun, Consuelo J. Perez, Peter Licence, David A. Barrett, and Demian R. Ifa.

Journal: Analytical Chemistry, Volume 87, Issue 6, Pages 3286-93. 2015.

DOI: 10.1021/ac5042445

Contributions: My contributions to this publication included participating in all of the experiments, data analysis and interpretation. Partial writing and editing of the introduction, results and discussion, created some figures for the manuscript and supporting information. Reviewed and edited the manuscript before submission to Analytical Chemistry. Participated in the modifications requested by the reviewers to the manuscript after submission to the journal.

Abstract

This work illustrates reactive desorption electrospray ionization mass spectrometry (DESI-MS) with a stable dication on biological tissues. Rat brain and zebra fish tissues were investigated with reactive DESI-MS in which the dictation forms a stable bond with biological tissue fatty acids and lipids. Tandem mass spectrometry (MS/MS) was used to characterize the dication (DC9) and to identify linked lipid-dication compounds formed. The fragment *m*/*z* 85 common to both DC9 fragmentation and DC9-lipid fragmentation was used to confirm that DC9 is indeed bonded with the lipids. Lipid signals in the range of *m*/*z* 250–350 and phosphoethanolamines (PE) *m*/*z* 700–800 observed in negative ion mode were also detected in positive ion mode with reactive DESI-MS with enhanced signal intensity. Reactive DESI-MS imaging in positive ion mode of rat brain and zebra fish tissues allowed enhanced detection of compounds commonly observed in the negative ion mode.

5. Publication #5: Analysis in Metabolic Changes in Plant Pathosystems by Imprint Imaging DESI-MS.

Authors: Alessandra Tata, Consuelo J. Perez, Tanam S. Hamid, Mark N. Bayfield, Demian R. Ifa.

Journal: Journal of the American Society for Mass Spectrometry, Volume 26, Issue 4, Pages 641-8. 2015.

DOI: 10.1007/s13361-014-1039-0

Contributions: My contributions to this publication included participating in most of the laboratory experiments. Created some figures and tables from the manuscript and supporting information. Reviewed and edited the manuscript before submission to the Journal of the American Society for Mass Spectrometry.

Abstract

The response of plants to microbial pathogens is based on the production of secondary metabolites. The complexity of plant-pathogen interactions makes their understanding a challenging task for metabolomics studies requiring powerful analytical approaches. In this paper, the ability of ambient mass spectrometry to provide a snapshot of plant metabolic response to pathogen invasion was tested. The fluctuations of glycoalkaloids present in sprouted potatoes infected by the phytopathogen *Pythium ultimum* were monitored by imprint imaging desorption electrospray ionization mass spectrometry (DESI-MS). After 8 d from the inoculation, a decrease of the relative abundance of potato glycoalkaloids α-solanine (*m/z* 706) and α-chaconine (*m/z* 722) was observed, whereas the relative intensity of solanidine (*m/z* 398), solasodenone (*m/z* 412), solanaviol (*m/z* 430), solasodiene (*m/z* 396), solaspiralidine (*m/z* 428), γ-solanine/γ-chaconine (*m/z* 412), β-solanine (*m/z* 706) and β-chaconine (*m/z* 722) increased. The progression of the disease, expressed by the development of brown necrotic lesions on the potato, led to the further decrease of all the glycoalkaloid metabolites. Therefore, the applicability of imprint imaging DESI-MS in studying the plant metabolites changes in a simple pathosystem was demonstrated with minimal sample preparation.

References

1. Andre Venter, M.N., R. Graham Cooks, *Ambient Desorption Ionization Mass Spectrometry.* Trends in Analytical Chemistry 2008. **27**(4): p. 284-290.
2. Takats, Z., et al., *Mass Spectrometry Sampling Under Ambient Conditions with Desorption Electrospray Ionization.* Science, 2004. **306**: p. 471-473.
3. Costa, A.B. and R. Graham Cooks, *Simulated splashes: Elucidating the mechanism of desorption electrospray ionization mass spectrometry.* Chemical Physics Letters, 2008. **464**(1-3): p. 1-8.
4. Pretti, C., et al., *Acute Toxicity of Ionic Liquids to the Zebrafish (Danio rerio).* Green Chem, 2006. **8**(3): p. 238-240.
5. Ifa, D.R., et al., *Quantitative Analysis of Small Molecules by Desorption Electrospray Ionization Mass Spectrometry from Polytetrafluoroethylene Surfaces.* Rapid Commun Mass Spectrom, 2008. **22**: p. 503-510.
6. Robert B. Cody, J.A.L., J. Michael Nilles, H. Dupont Durst, *Direct Analysis in Real Time (DART) Mass Spectrometry.* JEOL news, 2005. **40**(1): p. 8-12.
7. Abraham K. Badu Tawiah, L.S.E., Zheng Ouyang, R. Graham Cooks, *Chemical Aspects of the Extractive Methods of Ambient Ionization Mass Spectrometry.* Annu. Rev. Phys. Chem, 2013. **64**: p. 481-505.
8. Andre Venter, P.E.S., R. Graham Cooks, *Droplet Dynamics and Ionization Mechanisms in Desorption Electrospray Ionization Mass Spectrometry.* Anal. Chem., 2006. **78**(8549-8555).
9. Harris, G.A., L. Nyadong, and F.M. Fernandez, *Recent Developments in Ambient Ionization Techniques for Analytical Mass Spectrometry.* Analyst, 2008. **133**(10): p. 1297-1301.
10. Takats, Z., J.M. Wiseman, and R.G. Cooks, *Ambient mass spectrometry using desorption electrospray ionization (DESI): instrumentation, mechanisms and applications in forensics, chemistry, and biology.* J Mass Spectrom, 2005. **40**(10): p. 1261-75.
11. Dill, A.L., et al., *Mass Spectrometric Imaging of Lipids using Desorption Electrospray Ionization.* J Chromatogr B Analyt Technol Biomed Life Sci, 2009. **877**(26): p. 2883-9.
12. Eberlin, L.S., et al., *Desorption Electrospray Ionization Mass Spectrometry for Lipid Characterization and Biological Tissue Imaging.* Biochim Biophys Acta, 2011. **1811**(11): p. 946-960.
13. Campbell, D.I., et al., *Improved Spatial Resolution in the Imaging of Biological Tissue using Desorption Electrospray Ionization.* Anal Bioanal Chem, 2012. **404**(2): p. 389-398.
14. Wu, C., et al., *Mass Spectrometry Imaging Under Ambient Conditions.* Mass Spectrom Rev, 2013. **32**(3): p. 218-243.
15. Manicke, N.E., et al., *Desorption Electrospray Ionization (DESI) Mass Spectrometry and Tandem Mass Spectrometry (MS/MS) of Phospholipids and Sphingolipids: Ionization, Adduct formation, and Fragmentation.* J Am Soc Mass Spectrom, 2008. **19**(4): p. 531-543.
16. Wiseman, J.M., et al., *Desorption Electrospray Ionization Mass Spectrometry: Imaging Drugs and Metabolites in Tissues.* Proc Natl Acad Sci USA, 2009. **105**(47): p. 18120-18125.
17. Mohana Kumara, P., et al., *Ambient Ionization Mass Spectrometry Imaging of Rohitukine, a Chromone Anti-Cancer Alkaloid, during Seed Development in Dysoxylum binectariferum Hook.f (Meliaceae).* Phytochemistry, 2015. **116**: p. 104-110.
18. Tata, A., et al., *Analysis of Metabolic Changes in Plant Pathosystems by Imprint Imaging DESI-MS.* J Am Soc Mass Spectrom, 2015. **26**(4): p. 641-648.
19. Cooks, R.G., et al., *New Ionization Methods and Miniature Mass Spectrometers for Biomedicine: DESI Imaging for Cancer Diagnostics and Paper Spray Ionization for Therapeutic Drug Monitoring.* Faraday Discuss, 2011. **149**: p. 247-267.

20. Takats, Z., et al., *Direct Trace Level Detection of Explosives on Ambient Surfaces by Desorption Electrospray Ionization Mass Spectrometry.* Chem Commun, 2005(15): p. 1950-1952.
21. Ifa, D.R., et al., *Forensic Analysis of Inks by Imaging Desorption Electrospray Ionization (DESI) Mass Spectrometry.* Analyst, 2007. **132**(5): p. 461-467.
22. Dill, A.L., et al., *Perspectives in Imaging using Mass Spectrometry.* Chem Commun 2011. **47**(10): p. 2741-6.
23. Vismeh, R., et al., *Localization and Quantification of Drugs in Animal Tissues by use of Desorption Electrospray Ionization Mass Spectrometry Imaging.* Anal Chem, 2012. **84**(12): p. 5439-5445.
24. Kertesz, V., et al., *Comparison of Drug Distribution Images from Whole-Body Thin Tissue Sections obtained using Desorption Electrospray Ionization Mass Spectrometry and Autoradiography.* Anal Chem, 2008. **80**: p. 5168-5177.
25. Olsen, L.R., et al., *Characterization of Midazolam Metabolism in Locusts: the Role of a CYP3A4-like Enzyme in the Formation of 1'-OH and 4-OH Midazolam.* Xenobiotica, 2015. **46**(2): p. 99-107.
26. Chramow, A., et al., *Imaging of Whole Zebrafish (Danio rerio) by Desorption Electrospray Ionization Mass Spectrometry.* Rapid Commun Mass Spectrom, 2014. **28**(19): p. 2084-2088.
27. Neumann, J., et al., *Biodegradability of 27 Pyrrolidinium, Morpholinium, Piperidinium, Imidazolium and Pyridinium Ionic Liquid Cations under Aerobic Conditions.* Green Chem, 2014. **16**(4): p. 2174-2184.
28. Weyershausen, B. and K. Lehmann, *Industrial Application of Ionic Liquids as Performance Additives.* Green Chem, 2005. **7**(1): p. 15-19.
29. Feijtel, T., et al., *Integration of Bioaccumulation in an Environmental Risk Assessment.* Chemosphere, 1997. **34**(11): p. 2337-2350.
30. Ventura, S.P., et al., *Toxicity Assessment of Various Ionic Liquid Families towards Vibrio fischeri Marine Bacteria.* Ecotoxicol Environ Saf, 2012. **76**(2): p. 162-168.
31. Ventura, S.P., et al., *Ecotoxicity Analysis of Cholinium-Based Ionic Liquids to Vibrio fischeri Marine Bacteria.* Ecotoxicol Environ Saf, 2014. **102**: p. 48-54.
32. Stolte, S., et al., *Effects of Different Head Groups and Functionalised Side Chains on the Aquatic Toxicity of Ionic Liquids.* Green Chem, 2007. **9**: p. 1170-1179.
33. Pretti, C., et al., *Acute Toxicity of Ionic Liquids for Three Freshwater Organisms: Pseudokirchneriella subcapitata, Daphnia magna and Danio rerio.* Ecotoxicol Environ Saf, 2009. **72**(4): p. 1170-1176.
34. Garcia, M.T., N. Gathergood, and P.J. Scammells, *Biodegradable Ionic Liquids : Part II. Effect of the Anion and Toxicology.* Green Chem, 2005. **7**(1): p. 9-14.
35. Bernot, R.J., et al., *Acute and Chronic Toxicity of Imidazolium-Based ILs on Daphnia magna.* Environ Toxicol Chem, 2005. **24**(1): p. 87-92.
36. Dumitrescu, G., et al., *Evaluation of the Acute Toxicity of Tetrabuthylammonium Bromide Ionic Liquid on the Histological Structure of Some Organs in Zebrafish (Danio rerio).* ACCL BIOFLUX, 2010. **3**(5): p. 404-414.
37. Pham, T.P., C.W. Cho, and Y.S. Yun, *Environmental Fate and Toxicity of Ionic Liquids: A Review.* Water Res, 2010. **44**(2): p. 352-372.
38. Benzagouta, M.S., et al., *Ionic Liquids as Novel Surfactants for Potential use in Oil Recovery.* Korean J Chem Eng, 2013. **30**(11): p. 2108-2117.
39. *Handbook of Green Chemistry: Green Processes* ed. P.T. Anastas. Vol. 9. 2014, Weiheim, Germany: Wiley-VCH Verlag GmbH & Co. KGaA. 572.
40. Ventura, S.P., et al., *Simple Screening Method to Identify Toxic/Non-Toxic Ionic Liquids: Agar Diffusion Test Adaptation.* Ecotoxicol Environ Saf, 2012. **83**: p. 55-62.
41. Ranke, J., et al., *Lipophilicity Parameters for Ionic Liquid Cations and their Correlation to in vitro Cytotoxicity.* Ecotoxicol Environ Saf, 2007. **67**(3): p. 430-438.

42. J. Arning, S.S., A. Boschen, F. Stock, W.R. Pitner, U. Welz-Biermann, B. Jastorff, and J. Ranke, *Quantatitive and Qualitative Structure Activity Relationships for the Inhibitory Effects of Cationic Head Groups, Functionalised Side Chains and Anions of Ionic Liquids on Acetylcholinesterase.* Green Chem, 2008. **10**: p. 47-58.
43. Geyer, H., G. Politzki, and D. Freitag, *Prediction of Ecotoxicological Behaviour of Chemicals.* Chemosphere, 1984. **13**(2): p. 269-284.
44. Arnot, J.A. and F.A.P.C. Gobas, *A Review of Bioconcentration Factor (BCF) and Bioaccumulation Factor (BAF) Assessments for Organic Chemicals in Aquatic Organisms.* Environ Rev, 2006. **14**(4): p. 257-297.
45. Manicke, N.E., et al., *High-throughput Quantitative Analysis by Desorption Electrospray Ionization Mass Spectrometry.* J Am Soc Mass Spectrom, 2009. **20**(2): p. 321-325.
46. Lostun, D., et al., *Reactive DESI-MS Imaging of Biological Tissues with Dicationic Ion-Pairing Compounds.* Anal Chem, 2015. **87**(6): p. 3286-3293.
47. Bell, M.V., R.J. Henderson, and J.R. Sargent, *The Role of Polyunsaturated Fatty Acids in Fish.* Comp Biohem Physiol, 1986. **83B**(4): p. 711-719.
48. Hansen, H.J.M., A.G. Olsen, and P. Rosenkilde, *Formation of Phosphatidylethanolamine as a Putative Regulator of Salt Transport in the Gills and Esophagus of the Rainbow Trout (Oncorhynchus mykiss).* Comp Biohem Physiol, 1995. **112B**(1): p. 161-167.
49. Coleman, D. and N. Gathergood, *Biodegradation Studies of Ionic Liquids.* Chem Soc Rev, 2010. **39**(2): p. 600-637.
50. Pisarova, L., et al., *Ionic Liquid Long-Term Stability Assessment and its Contribution to Toxicity and Biodegradation Study of Untreated and Altered Ionic Liquids.* P I Mech Eng J J Eng, 2012. **226**(11): p. 903-922.
51. Bonn, B., et al., *The molecular basis of CYP2D6-mediated N-dealkylation: balance between metabolic clearance routes and enzyme inhibition.* Drug Metab Dispos, 2008. **36**(11): p. 2199-2200.
52. Alderton, W., et al., *Accumulation and Metabolism of Drugs and CYP Probe Substrates in Zebrafish Larvae.* Xenobiotica, 2010. **40**(8): p. 547-557.
53. Erkog, F.U. and R.E. Menzer, *Metabolism of Trifluralin in Rats.* J. Agri. Food Chem., 1985. **33**: p. 1061-1070.
54. Rombough, P., *Gills are needed for Ionoregulation before they are needed for O2 uptake in Developing Zebrafish, Danio rerio.* J Exp Bio, 2002. **205**: p. 1787-1794.
55. Menke, A.L., et al., *Normal Anatomy and Histology of the Adult Zebrafish.* Toxicol Pathol, 2011. **39**(5): p. 759-775.
56. Jeong, J.Y., et al., *Functional and Developmental Analysis of the Blood-Brain Barrier in Zebrafish.* Brain Res Bull, 2008. **75**(5): p. 619-628.
57. Lockman, P.R. and D.D. Allen, *The Transport of Choline.* Drug Dev Ind Pharm, 2002. **28**(7): p. 749-771.
58. Jin, Y., et al., *Hepatic and extrahepatic expression of estrogen-responsive genes in male adult zebrafish (Danio rerio) as biomarkers of short-term exposure to 17beta-estradiol.* Environ Monit Assess, 2008. **146**(1-3): p. 105-11.
59. Douglas, K.A., Jain, S., Brant, W.R. Venter, A.R., *Deconstructing Desorption Electrospray Ionization: Independant Optimization and Ionization by Spray Desorption Collection.* Journal of the American Society for Mass Spectrometry, 2012. **23**(11): p. 1896-902.
60. Ellis, S.R., A.L. Bruinen, and R.M.A. Heeran, *A Critical Evaluation of the Current State-of-the-Art in Quantitative Imaging Mass Spectrometry.* Anal Bioanal Chem, 2014. **406**: p. 1275-1289.

Appendix

A. ESI-MS/MS Spectra of AMMOENG 130 from a Hybrid LTQ-Orbitrap Mass Spectrometer

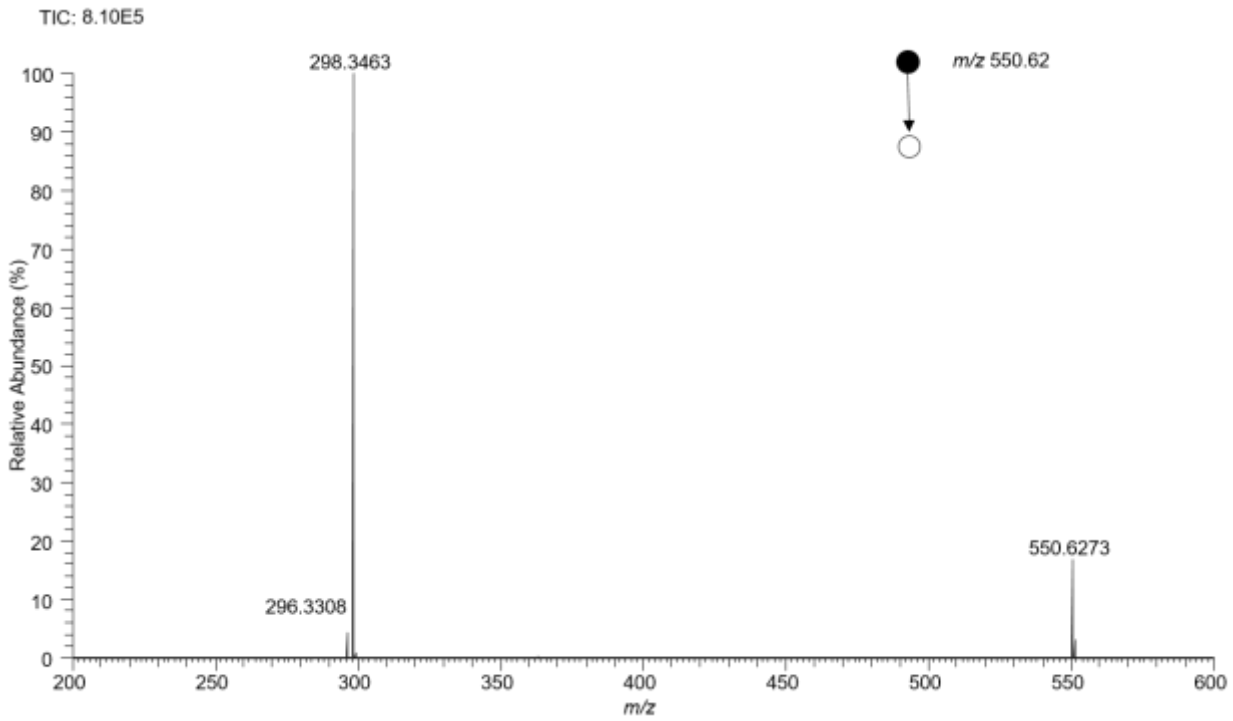

Figure A1: ESI-MS/MS Spectra of AMMOENG 130 (distearyldimethylammonium ion) of *m/z* 550.6273 with a mass error of 3.3 ppm. CID fragments in the spectra correspond to $[C_{21}H_{44}N]^+$ of *m/z* 298.3456 and $[C_{20}H_{42}N]^+$ of *m/z* 296.3308 using a collision energy of 48 a.u.

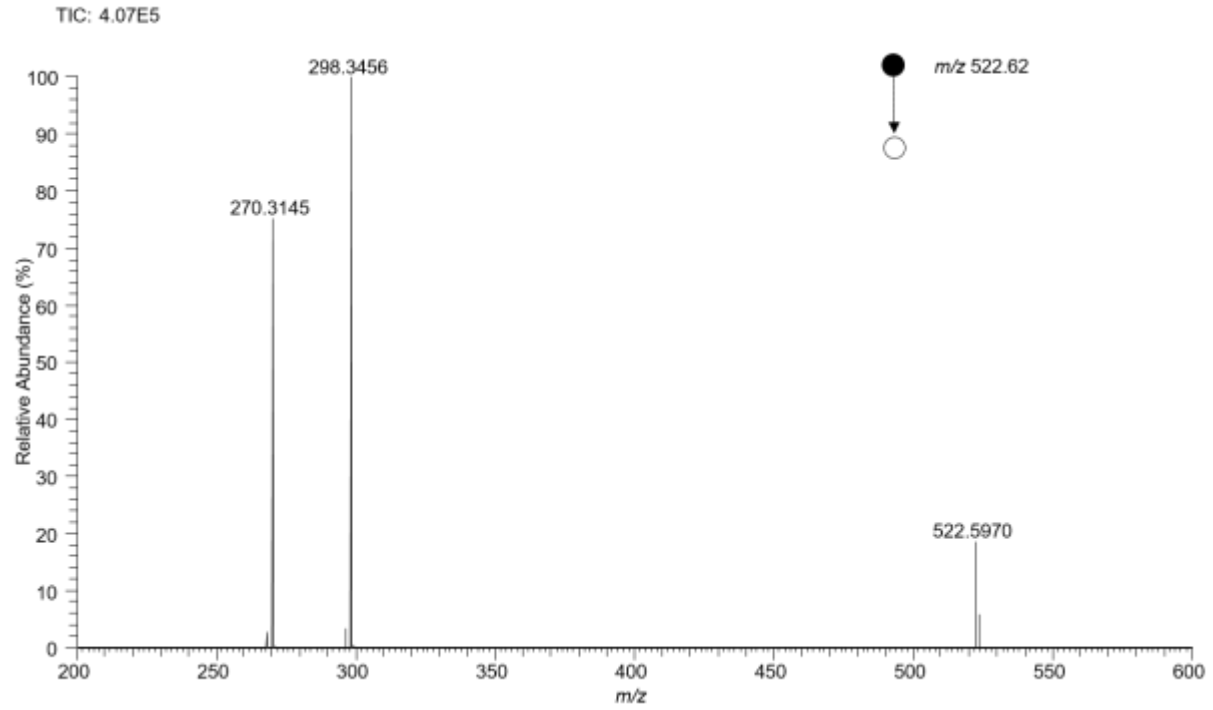

Figure A2: ESI-MS/MS Spectra of Hexadecylstearyldimethylammonium ion of *m/z* 522.6267 with a mass error of 4.5 ppm. CID fragments in the spectra correspond to $[C_{21}H_{44}N]^+$ of *m/z* 298.3456 and $[C_{20}H_{42}N]^+$ of *m/z* 270.3145 using a collision energy of 50 a.u.

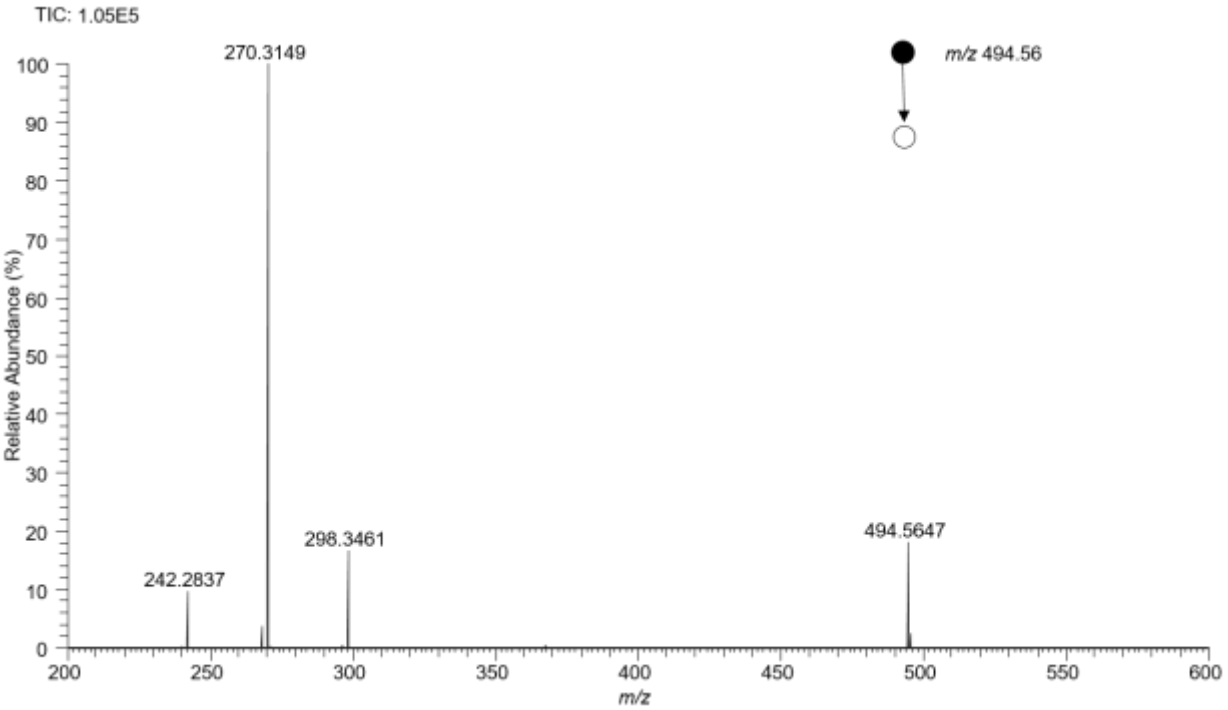

Figure A3: ESI-MS/MS Spectrum of Tetradecylstearyldimethylammonium ion/ Dihexadecyldimethylammonium ion of *m/z* 494.5647 with a mass error of 3.6 ppm. CID fragments in the spectrum using a collision energy of 48 a.u. gave rise to fragments of *m/z* 270.3149, *m/z* 298.3461 and *m/z* 242.2837 corresponding to $[C_{21}H_{44}N]^+$, $[C_{20}H_{42}N]^+$, and $[C_{16}H_{36}N]^+$, respectively.

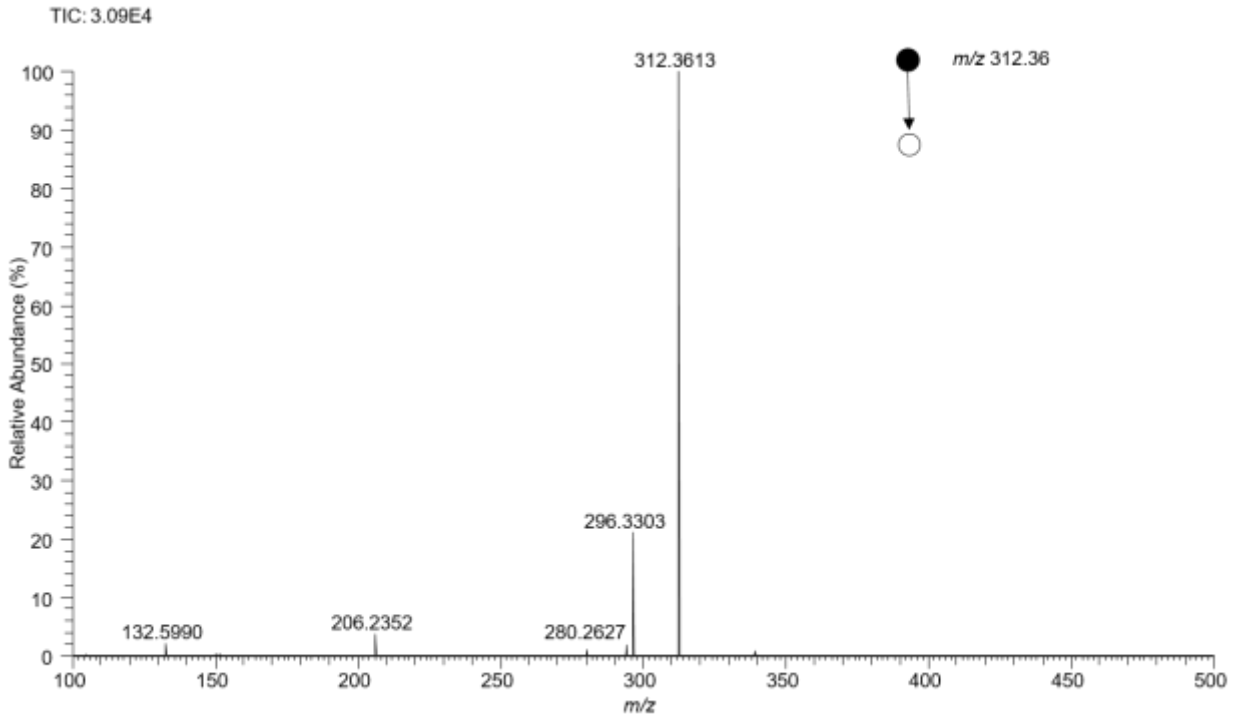

Figure A4: ESI-MS/MS spectrum of Stearyltrimethylammonium ion of *m/z* 312.3613 with a mass error of 1.7 ppm. CID fragments in the spectrum were produced using a collision energy of 45 a.u. giving rise to fragments of *m/z* 296.3303 corresponding to $[C_{20}H_{42}N]^+$ and other fragments of *m/z* 280.2627, *m/z* 206.2352 and *m/z* 132.5990.

B. ESI-MS Spectra of AMMOENG 130 Degradation in Water in Time Intervals between 0-96 hours

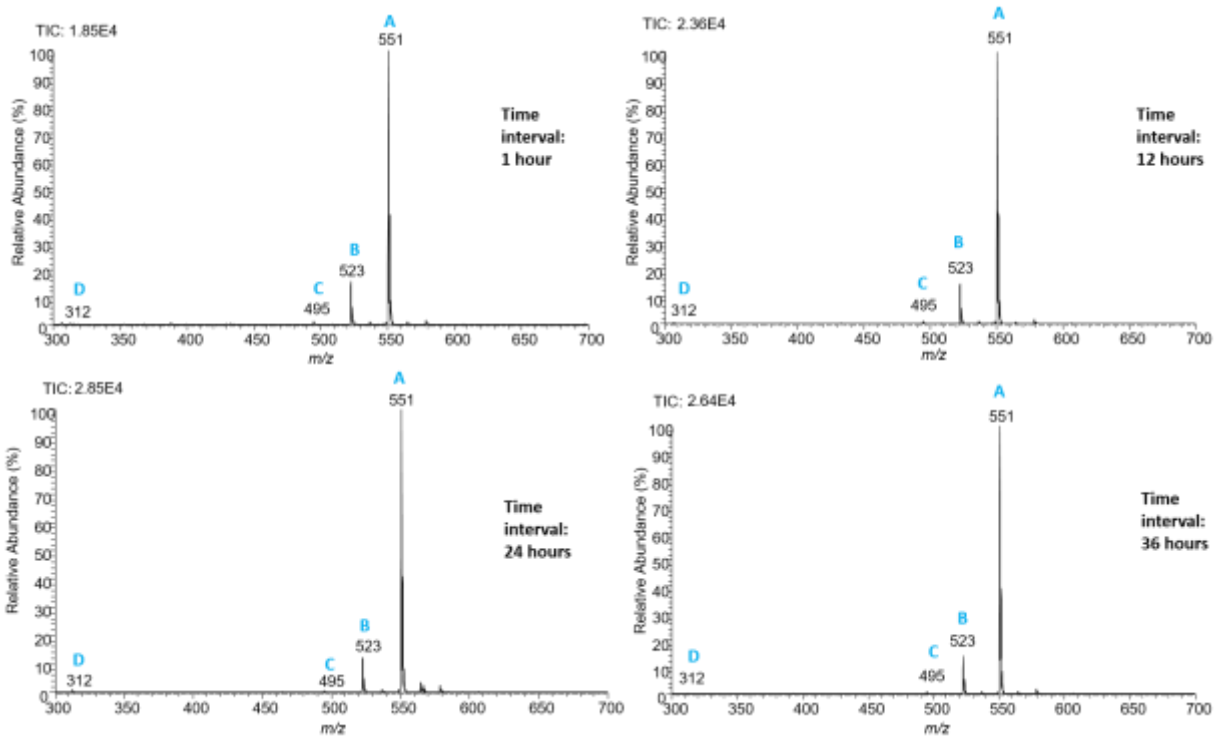

Figure B1: ESI-MS spectrum of AMMOENG 130 in water at a concentration of 1.25 mg/L after 1 hour, 12 hours, 24 hours and 36 hours in a mass range of *m/z* 300-700.

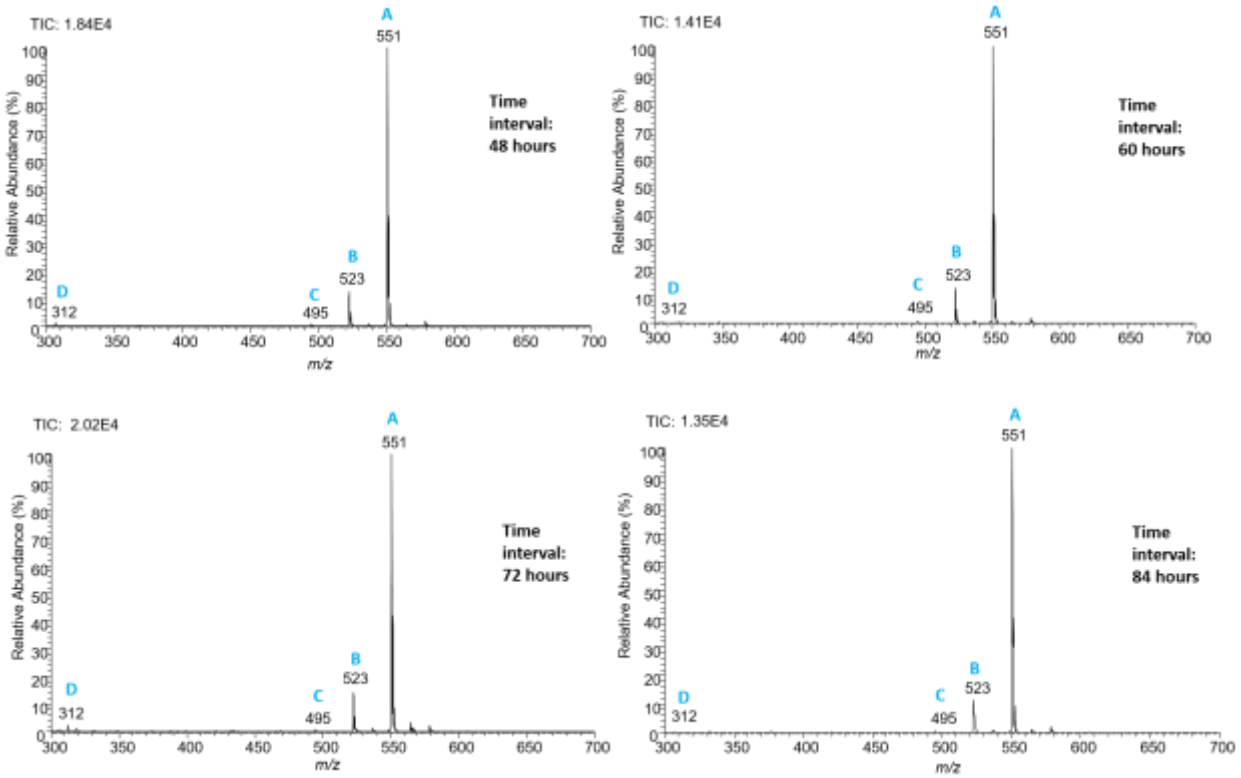

Figure B2: ESI-MS spectrum of AMMOENG 130 in water at a concentration of 1.25 mg/L after 48 hours, 60 hours, 72 hours and 84 hours in a mass range of *m/z* 300-700.

C. ESI-MS Spectrum of AMMOENG 100

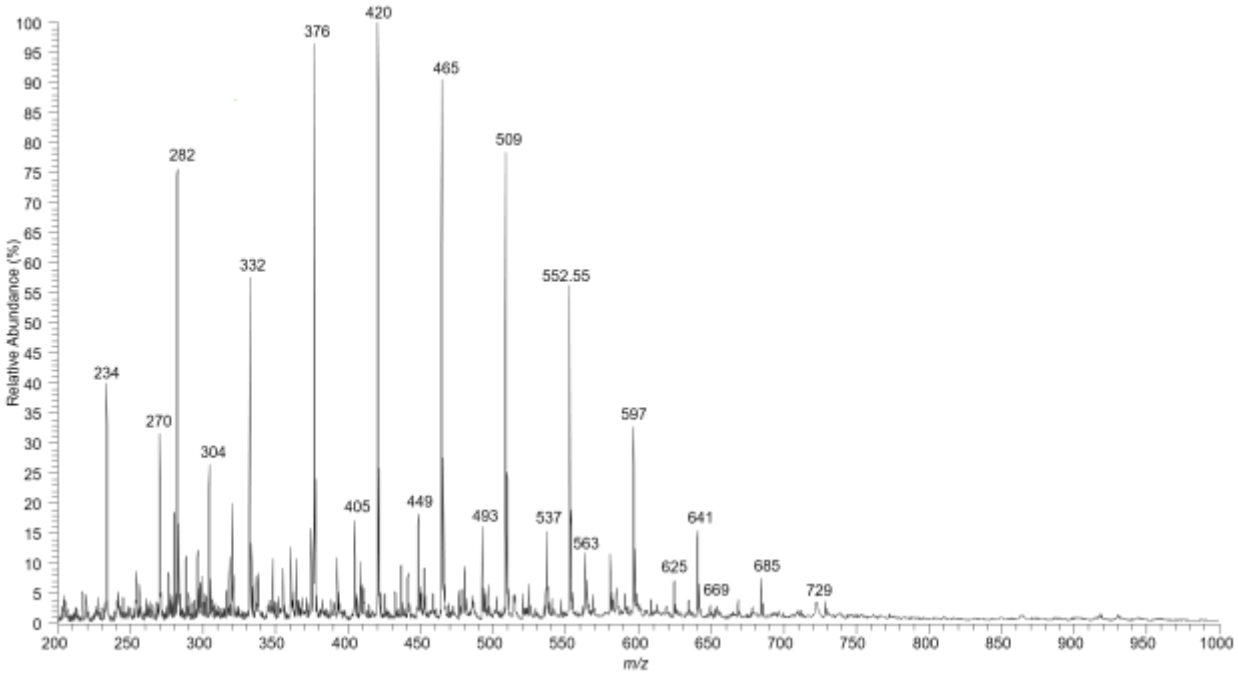

Figure C1: ESI-MS spectrum of a standard solution of AMMOENG 100 in positive ion mode at a concentration of 100 ng/mL.